

Fall 12-1985

Absorption Cross-Sections of Sodium Diatomic Molecules

Zeng-Shevan Fong
Old Dominion University

Follow this and additional works at: https://digitalcommons.odu.edu/physics_etds



Part of the [Atomic, Molecular and Optical Physics Commons](#)

Recommended Citation

Fong, Zeng-Shevan. "Absorption Cross-Sections of Sodium Diatomic Molecules" (1985). Master of Science (MS), Thesis, Physics, Old Dominion University, DOI: 10.25777/qgb9-wz86
https://digitalcommons.odu.edu/physics_etds/194

This Thesis is brought to you for free and open access by the Physics at ODU Digital Commons. It has been accepted for inclusion in Physics Theses & Dissertations by an authorized administrator of ODU Digital Commons. For more information, please contact digitalcommons@odu.edu.

ABSORPTION CROSS-SECTIONS
OF SODIUM DIATOMIC MOLECULES

by

Zeng-Shevan Fong
B.S. June 1980, Tamkang University, Taiwan, R.O.C.

A Thesis Submitted to the Faculty of
Old Dominion University in Partial Fulfillment of the
Requirements for the Degree of

MASTER OF SCIENCE

PHYSICS

OLD DOMINION UNIVERSITY
December, 1985

Approved by:

Wynford Harries

James L. Cox, Jr.

G. E. Copeland

Mark D. Havey

G. R. Hoy

ABSTRACT

ABSORPTION CROSS-SECTIONS OF SODIUM DIATOMIC MOLECULES

Zeng-Shevan Fong
Old Dominion University, 1985
Thesis Advisor: Dr. Wynford L. Harries

The absorption cross-sections of sodium dimers have been studied using a "heat-pipe" oven operating in the "non-heat-pipe" mode. Three wavelength regions were observed. They are in the red ($A^1 \Sigma_u^+ - X^1 \Sigma_g^+$), in the green-blue ($B^1 \Pi_u - X^1 \Sigma_g^+$), and in the near ultraviolet regions ($C^1 \Pi_u - X^1 \Sigma_g^+$). The absorption cross-section depends on the wavelength of the incident light. Representative peak values for the $v''=0$ progression in the red ($A \leftarrow X$ transitions) and green-blue ($B \leftarrow X$ transitions) regions are 2.59 \AA^2 (average value) and 11.77 \AA^2 ($T_{\text{ave}}=624^\circ\text{K}$). The value for the $C \leftarrow X$ transitions is several tenths \AA^2 . The cross-sections were measured from absorption spectra taken as a function of temperature.

In comparison with published results, our values agree with the paper by L. K. Lam and his co-workers, they agree approximately with the paper by R. D. Hudson but are in disagreement with the paper by M. A. Henesian.

ACKNOWLEDGMENTS

I wish to express my sincerest gratitude to Professor Wynford L. Harries of the Old Dominion University for his instruction and guidance. I am also grateful to Dr. Nelson Jalufka of NASA for his valuable advice and discussion on experiment and theory, and to Mr. Al Bond of NASA for his able technical assistance. My thanks are also due to NASA for their financial aid from Grant NSG 1568, Professor Harries Principal investigator, and for providing me with an excellent experimental environment.

TABLE OF CONTENTS

	Page
Acknowledgments	ii
List of Tables	iv
List of Figures	v
 Chapter	
I Introduction	1
II Theory	5
The hydrogen molecule and the hydrogen-like molecules	6
Anharmonic vibrations of diatomic molecules	10
Molecular transitions	11
Franck-Condon factors	13
III Experiment	19
Apparatus	22
Calibration	27
Experimental process	28
IV The calculation of the absorption cross-sections	33
V Discussion and Conclusion	58
Bibliography	63
Appendix A	65
Appendix B	66
Appendix C	68

List of Tables

Table	page
1. For $v''=0$, absorption cross-sections of $A \leftarrow X$ (\AA^2) transitions under the pressure of buffer gas, helium, 20 torr	56
2. For $v''=0$, absorption cross-sections of $A \leftarrow X$ (\AA^2) transitions under the pressure of buffer gas, helium, 30 torr	56
3. For $v''=0$, absorption cross-sections of $B \leftarrow X$ (\AA^2) transitions under the pressure of buffer gas, helium, 20 torr	57
4. For $v''=0$, absorption cross-sections of $B \leftarrow X$ (\AA^2) transitions under the pressure of buffer gas, helium, 30 torr	57
5. For $v''=0$, absorption cross-sections of $C \leftarrow X$ (\AA^2) transitions under the pressure of buffer gas, helium, 30 torr	57

List of Figures

Figure	page
1. The hydrogen molecule. The protons are in positions A and B; the electrons, in 1 and 2	7
2. Electronic energy levels. The energy is given as a function of the internuclear distance r_{AB} for three different electronic states, E_1 , E_2 , E_3 . E_1 and E_3 correspond to stable configuration. The equilibrium distance and the electron binding energy in the ground state are indicated, respectively, by r_e and D_e	9
3. Possible dependence on the distance between the nuclei of the energy of two electronic states of a diatomic molecule	14
4. Heat-pipe used in experimental studies	20
5. The total pressure of sodium vapor (dotted curve) and the partial pressure of sodium diatoms (solid curve) are functions of temperature. The experimental data is taken from reference [21]	21
6a. Experimental arrangement designed to study the absorption cross-sections of sodium dimers.	23
6b. Experimental setup for measuring the absorption cross-sections of sodium dimers.	24
7. Mercury light spectrum from 300 nm to 420 nm (for calibration use)	29
8. Mercury light spectrum from 430 nm to 550 nm (for calibration use)	30
9. Mercury light spectrum from 560 nm to 680 nm and scan 4 times (for calibration use).	31
10. The absorption spectra taken under helium pressure 20 torr and input power 162 watts. \bar{n} (average sodium dimer density) x L (optical	

path)= 8.713×10^{14} . The hand drawn curves are the background	34
11. The absorption spectrum taken under helium pressure 20 torr and input power 162.5 watts. \bar{n} (average sodium dimer density)x L (optical path)= 8.133×10^{14} . The hand drawn curve is the background	35
12. The absorption spectra taken under helium pressure 20 torr and input power 192 watts. \bar{n} (average sodium dimer density)x L (optical path)= 2.24×10^{15} . The hand drawn curves are the background	36
13. The absorption spectrum taken under helium pressure 20 torr and input power 192 watts. \bar{n} (average sodium dimer density)x L (optical path)= 2.24×10^{15} . The hand drawn curve is the background	37
14. The absorption spectra taken under helium pressure 30 torr and input power 152.5 watts. \bar{n} (average sodium dimer density)x L (optical path)= 3.65×10^{14} . The hand drawn curves are the background	38
15. The absorption spectra taken under helium pressure 30 torr and input power 165 watts. \bar{n} (average sodium dimer density)x L (optical path)= 9.87×10^{14} . The hand drawn curves are the background	39
16. The absorption spectrum taken under helium pressure 30 torr and input power 185 watts. \bar{n} (average sodium dimer density)x L (optical path)= 3.05×10^{15} . The hand drawn curve is the background	40
17. The absorption spectrum taken under helium pressure 30 torr and input power 185 watts. \bar{n} (average sodium dimer density)x L (optical path)= 3.05×10^{15} . The hand drawn curve is the background	41
18. The absorption spectrum taken under helium pressure 30 torr and input power 185 watts. \bar{n} (average sodium dimer density)x L (optical path)= 3.05×10^{15} . The hand drawn curve is the background	42

19. The absorption spectra taken under helium pressure 30 torr and input power 207 watts. \bar{n} (average sodium dimer density) \times L (optical path)= 5.88×10^{15} . The hand drawn curves are the background	43
20. The absorption spectrum taken under helium pressure 30 torr and input power 212 watts. \bar{n} (average sodium dimer density) \times L (optical path)= 5.88×10^{15} . The hand drawn curve is the background	44
21. The error percentage of equation (20) versus temperature.	47
22. Calculated temperature profiles for the heat-pipe at helium pressure of 20 torr and 125 watts, input power. For $r=1.27$ cm, $r=0.5$ cm, and $r=0$ cm (r is semidiameter), we get three curves, the upper, the middle, and the lower	48
23. Relative populations of the vibrational energy levels for Na_2 gas at 500°K	51
24. Absorption cross-section versus temperature. The points around the solid line are the absorption cross-section for $A \leftarrow X$ transitions at wavelength, 628.8 nm and the points around the dashed line are the absorption cross-section for $B \leftarrow X$ transitions at wavelength, 486.7 nm.	59
25. Plot of σ_{abs} ($B \leftarrow X$) versus wavelength for Na_2 at $T_{\text{ave}}=624^\circ\text{K}$ for the transitions $v''=0$ to $v'=0$ to 6.	61

CHAPTER I

INTRODUCTION

The study of solar pumped lasers was started by C. G. Young in early 1965 [1]. The purpose for these studies is to use large solar collectors on orbiting space stations which transmit the collected energy using laser beams to the earth or to other vehicles in space missions. The goal of the research is to determine if the solar energy could be converted directly into laser radiation, then the inefficiencies in converting the energy through different transducers could be avoided. Hence broadband optical pumping or photon excitation methods for producing the population inversion necessary for optical amplification are investigated. The major fraction of the solar spectrum lies in the long wavelength (visible) region with a peak at about 2 eV, and the laser medium should have a good absorption efficiency in this wavelength region. Gas lasers would be advantageous because of uniform media, and their volume could be large (in space applications, the size of the laser would not be critical), and they are easily constructed. Here the possibility of using sodium vapor as the medium for solar pumped gas lasers used as energy converters is examined.

To convert solar energy by a gas laser the following candidates have been recently considered: I_2 , Br_2 , Br_2-CO_2-He , IBr ,

C_3F_7I ...etc.. Two kinds of lasers were studied theoretically. In the first category: the absorber and the lasant were different materials such as a Br_2-CO_2-He laser. (the Br_2 absorbed the photons and transferred the energy to CO_2 , which lased) In the second category: only one material was used, such as an IBr laser; however, the theoretical solar power efficiencies in these cases were low (0.5 and 1.2 percent respectively) [2].

In the above cases, the absorbed photons produced excited atoms Br^* or I^* (photo-dissociation) which then lased to the ground atomic level, but there are not many diatomic molecules that can be dissociated by light near the solar peak (around 450nm-550nm). The requirement of photo-dissociation limits their absorbed wavelength range, resulting in a reduction in their efficiencies. However, there are a great many that can absorb a photon and then be raised to one of the vibration-rotational levels of an upper electronic state without dissociation. Lasing could then occur as a transition to one of the vibration-rotational levels of the ground electronic states. Recently a number of optically pumped dimer lasers (bound-bound) were listed including the metal vapors Li_2 , Na_2 , K_2 , Bi_2 , and Te_2 which lased without dissociation [3] [4].

Alkali metal vapors interact very strongly with light particularly in the visible region near the peak solar spectrum. Lasers made from these vapors have low thresholds and high measured efficiencies and because absorption will occur near the peak of the solar spectrum, the possibility of using these vapors as solar energy converters arises. The quoted device efficiencies were up to 15 percent [3], but for solar energy conversion the overall efficiency

should include the solar efficiency (fraction of the solar radiance used) which is usually below 20 percent [5]. Vaporizing the metals would be achieved by solar concentrators and the lasers would run at temperatures of around 1000°K. The high temperature would also reduce the area requirement of the heat dissipation surface, an important factor in the output power to weight ratio [6], and an advantage over the IBr [2], I₂, and Br₂ lasers. The dimer/monomer ratios of alkali metal vapors are functions of temperature and the ratio for sodium vapor is the highest of all under certain temperatures [7]. In view of the above considerations sodium is a good candidate for the medium of a solar pumped laser.

For the satisfactory operation of a laser system, the self-absorption should also be low. This restricts the choice of molecules and transitions as self-absorption becomes a particularly important loss mechanism for emission from higher molecular bands. Hence the emission wavelength should be chosen where there is little self-absorption. Previous studies [3] [4] have shown that this is possible for sodium. It is important to measure the absorption spectra for sodium vapor, and also to obtain absorption cross-sections for kinetic studies.

However for kinetic studies it is essential for the absolute value of the cross-sections (as functions of wavelength) be known. Here the literature shows violet disagreement. L. K. Lam, A. Gallagher and M. M. Hessels' data show values of the $A^1\Sigma_u^+ - X^1\Sigma_g^+$ to be 10^{-16} cm² [8], whereas M. A. Hennesian, R. L. Herbst and R. L. Byers' results show values of 10^{-12} cm² [9]. It is therefore essential to measure the absolute values.

As results of our experimental data showing the absorption spectra measured with a heat-pipe operated in non-heat-pipe mode, the absorption cross-section $A^1 \Sigma_u^+ - X^1 \Sigma_g^+$ was obtained with a magnitude of the right order $\sim 10^{-16} \text{ cm}^2$ and $B^1 \Pi_u - X^1 \Sigma_g^+$ was around $\sim 10^{-15} \text{ cm}^2$ and $C^1 \Pi_u - X^1 \Sigma_g^+$ was around $\sim 10^{-17} \text{ cm}^2$. The absorption cross-sections for these bands are large compared with I_2 , Br_2 , $\text{C}_3\text{F}_7\text{I}$, and IBr , whose absorption cross-sections are $\sim 10^{-19} \text{ cm}^2$ [5]. The experiments also showed that photo-dissociation occurred easily. These reasons increase the potential of sodium metal vapor, as the material for a solar pumped laser.

CHAPTER II

THEORY

Before we examine molecules let us first consider a collection of identical atoms having two electronic levels each. In the case of atoms there are three processes concerned with electron transitions between two electronic energy levels. The first is absorption of a photon by an atom in the ground state which simultaneously undergoes a transition to an excited state. The absorbing frequency is determined by the energy difference ΔU between the excited state and ground state, $\Delta U = h\nu$. The second process is spontaneous emission of a photon from an excited atom as it returns to the ground state. The third is the stimulated emission of a photon from an excited atom which is caused to return to the ground state by an electromagnetic wave of frequency corresponding to the transition frequency. Both the original and emitted photons are coherent and also become the source to induce other excited atoms. The most important process in laser action is the third example mentioned. If there are many atoms in excited states, the stimulated emission can increase the intensity of radiation of the transition frequency with all the photons in the same phase. This is the principle of laser action in atomic lasers.

The process of lasing is similar for molecules and atoms.

However the case of atomic lasers, their quantum efficiencies are low. Much higher quantum efficiencies can be obtained with molecular lasers, essential for energy conversion using solar pumped lasers. A molecule has many energy levels, and to study the transitions between those energy levels, we study the absorption spectra of molecules which can help us design a dimer laser.

1. The hydrogen molecule and the hydrogen-like molecules:

The theoretical simplicity of the alkali metal atoms (one electron outside an inert ionic core) and molecules (two electrons outside two inert ionic cores) makes them even more ideal; in a sense they are "visible hydrogen atoms and molecules [10]."

Let us consider first the hydrogen molecule. It is composed of four particles, two protons (A and B) and two electrons (1 and 2) (see Figure 1.). To determine the energy of the electrons in a molecule for fixed values of the nuclear coordinates, that is in the adiabatic approximation, the potential energy appearing in the Schrodinger's equation must take into account all the electrostatic interactions between the four charged particles. The potential is

$$U = -e^2 \left[\frac{1}{r_{1A}} + \frac{1}{r_{2A}} + \frac{1}{r_{1B}} + \frac{1}{r_{2B}} - \frac{1}{r_{12}} - \frac{1}{r_{AB}} \right] \quad (1)$$

Fortunately, it is possible to simplify the problem by using the approximate method of Born and Oppenheimer [11]. It states that the complete wave function can be expressed as a product of the electronic wave function and the nuclear wave function. The

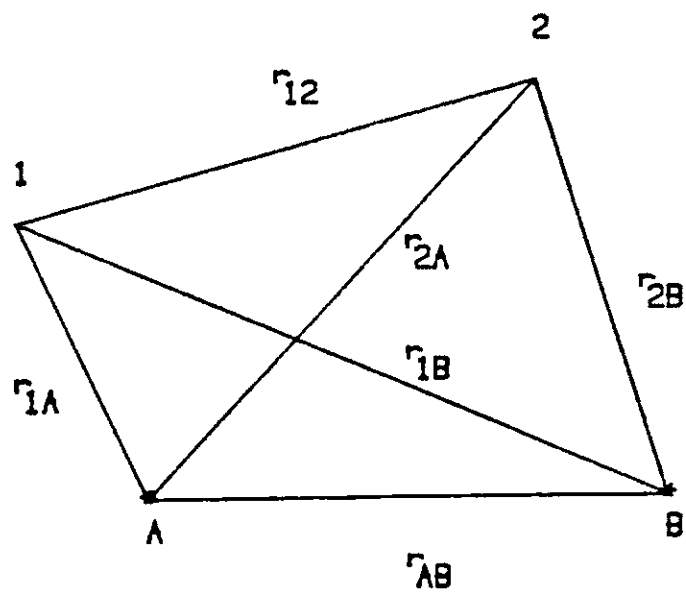


Figure 1. The hydrogen molecule. The protons are in positions A and B; the electrons, in 1 and 2.

electronic wave function depends on the position of the nuclei, but not on their state of motion. The nuclear wave function depends on the whole electronic configuration. The total energy of the molecule may be expressed, to a first approximation by the sum of a nuclear energy term and an electronic one. The electronic energy is quantized as the electronic wave function. It depends also on the position of the nuclei; the coordinates of the nuclei are present as parameters in the expression of each electronic level. In the hydrogen molecule there are six such coordinates. But if we are interested only in the relative position of the nuclei, and not in their absolute position in space, a single parameter suffices—namely the internuclear distance r_{AB} . The potential energy curves, for the atoms in a center of mass system as functions of r_{AB} and their variation follows the general pattern schematically represented in Figure 2.. Curves E_1 and E_3 of Figure 2. have a minimum in their energy; in other cases (like E_2) there is no minimum. Curves E_1 and E_3 correspond to two outer electrons where the spins are anti-parallel and therefore must be symmetric, and the spin states of the electrons is the singlet. Curves E_2 corresponds to two electrons whose spins are parallel and therefore must be anti-symmetric and the spin state of the electrons is the triplet state. In E_3 there is one electron in the first excited state. A value of the equilibrium internuclear distance r_e and of the dissociation energy D_e , two very important structural parameters of the molecule are indicated. The same considerations apply to the Na_2 molecule.

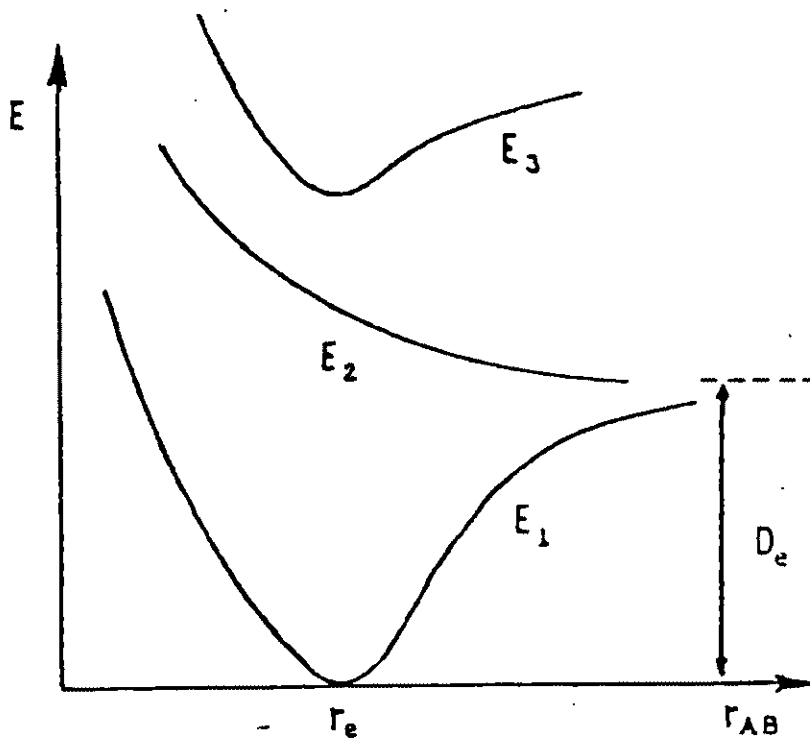


Figure 2. Electronic energy levels. The energy is given as a function of the internuclear distance r_{AB} for three different electronic states, E_1 , E_2 , E_3 . E_1 and E_3 correspond to stable configuration. The equilibrium distance and the electron binding energy in the ground state are indicated, respectively, by r_e and D_e .

2. Anharmonic vibrations of diatomic molecules:

The exact form of the potential curve governing the vibrational motion of the nuclei may be calculated. It is the electronic energy introduced by the Born-Oppenheimer theorem. It may also be constructed, point for point, from the observed vibrational and rotational levels. The Morse function $U=D_e[1-e^{-B(r-r_e)}]^2$ [12] is an acceptable approximation of the actual potential curve of a diatomic molecule of type E_1 , except for $r=0$ where it has a finite value and the true potential is infinite. For $r=r_e$ the equation becomes zero: this is the minimum value of the potential energy and occurs at the equilibrium position. When $r \rightarrow \infty$, U approaches D_e , which is consequently the dissociation energy. There are three parameters D_e , r_e , and B which determine the shape of a molecular potential curve. If the true potential is known, they will be adjusted to give the best overlap with the true potential. After the parameters D_e , r_e , and B are calculated, it is possible to find an exact solution to the wave equation for the vibrational energy levels of the molecule which are

$$G(v)=W_e(v+1/2)-W_eX_e(v+1/2)^2+\dots \quad (2)$$

where v is the vibrational quantum number and W_e is the zero-order vibrational frequency and W_eX_e is the anharmonicity constant. W_e and W_eX_e are related to D_e and B as follows:

$$W_e=(B/2\pi c) \cdot (2D_e/\mu)^{1/2} \quad (3)$$

$$W_e X_e = hB^2 / (8\pi^2 \mu c) \quad (4)$$

where h is Planck's constant and μ is the reduced mass of the diatom and c is the speed of light. The parameters D_e and B can be calculated when W_e and $W_e X_e$ are known. Values of sodium dimer are given in Molecular Spectra and Molecular Structure IV. Constants of Diatomic Molecules [13].

3. Molecular transitions:

A molecule, just as an atom, has many electronic levels corresponding to different distributions of the electrons over their various orbitals and to different orientations of the electronic angular momenta. The spectra that arise in transitions from one electronic state to another are a series of lines which result from nuclear vibration and rotation.

The energy of the molecule may be written as the sum of three contributions: electronic, vibrational, and rotational, that is

$$E_{\text{total}} = E_e + E_v + E_r \quad (5)$$

or, in term values,

$$T = E_{\text{total}} / hc = T_e + G(v) + F_v(J) \quad (6)$$

where T and the other quantities are expressed in cm^{-1} .

For an electronic transition of a diatomic molecule we have

$$\Delta U = T' - T'' = \Delta U_e + \Delta U_v + \Delta U_r \quad (7)$$

where the "single prime", T' and the "double prime", T'' are respectively the upper and lower energy levels of a diatomic molecule with different electronic, vibrational, and rotational energies.

$$\Delta U_e = T'_e - T''_e, \quad \Delta U_v = G'(v') - G''(v'') \quad (8)$$

$$\Delta U_r = F'_{v'}(J') - F''_{v''}(J'')$$

If we consider one particular electronic transition with ΔU_e fixed, then all possible values of ΔU_r and ΔU_v give rise to a band system. The gaps between vibrational levels are much larger than the gaps between rotational levels and the typical values for a sodium dimer for the rotational gaps are around $\sim 0.5 \text{ cm}^{-1}$ and for the vibrational gaps are around $\sim 150 \text{ cm}^{-1}$. Under low resolution we can to a first approximation neglect ΔU_r and obtain for the bands of an electronic band system of a diatomic molecule

$$\begin{aligned} \Delta U = & \Delta U_e + W_e'(v'+1/2) - W_e X_e'(v'+1/2)^2 + \dots \\ & - [W_e''(v''+1/2) - W_e X_e''(v''+1/2)^2 + \dots] \quad (9) \end{aligned}$$

the band system can be considered either as consisting of a number of v' progressions or of a number of v'' progressions. Unlike the harmonic oscillator, there is no restrictive selection rule for the

vibrational quantum number v' . The wave numbers will give a great number of bands, when v' and v'' are replaced by arbitrary non-negative integers. However the absorption or emission of a photon can only occur if the probability of the transition is high, for a given v' , v'' . To start determining the value of the level of v'' , we need to consider the Franck-Condon principle.

4. Franck-Condon factors:

The Franck-Condon principle [14] starts from the assumption that because of the large difference between the nuclear and the electronic masses, that the electronic transition takes place so rapidly, that the nuclei in the molecule cannot alter their relative positions nor their relative velocities significantly. Since the nuclei move in different potential fields in different electronic states, the transition of the electrons to a new state is usually accompanied by a subsequent change in the equilibrium positions of the nuclei -and the frequencies of the normal vibrations- and this leads to the simultaneous excitation of electronic and vibrational states. The character of such excitations is determined by the dependence of the electronics states of the molecule on the arrangement of the nuclei. For the simplest case, the potential energy of diatomic molecules depends on only one coordinate: the distance between the nuclei.

We have depicted qualitatively in Figure 3. the possible dependence on the distance between the nuclei of the energy of a

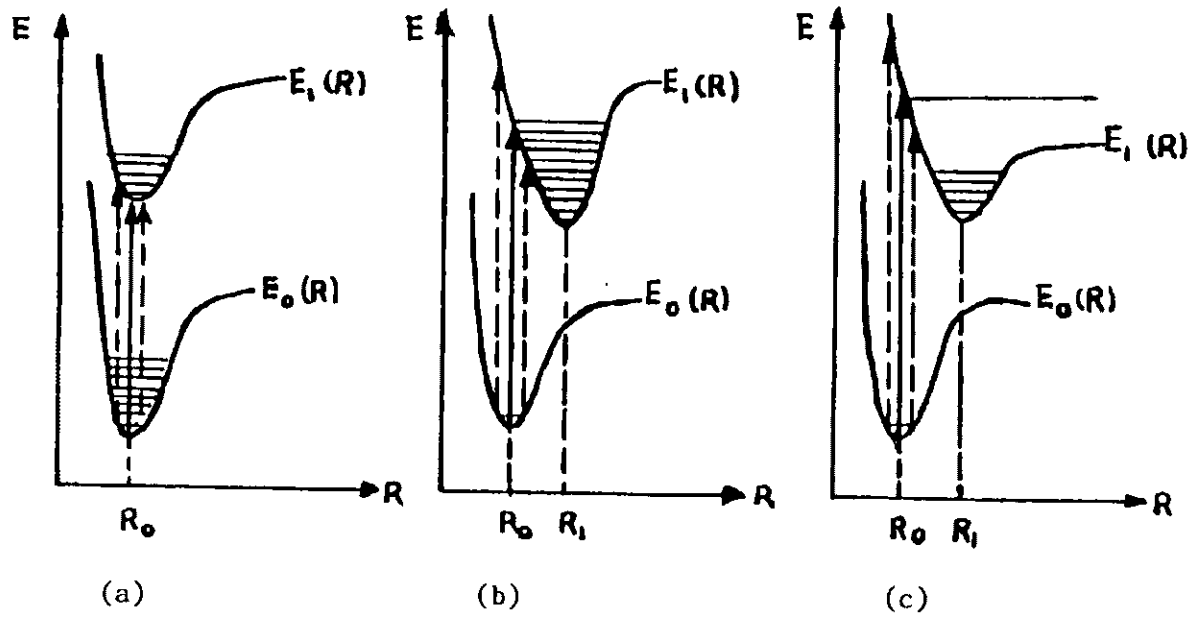


Figure 3. Possible dependence on the distance between the nuclei of the energy of two electronic states of a diatomic molecule.

diatomic molecule for two electronic states. Case (a) corresponds to two electronic states for which the minima of the functions $E_0(R)$ and $E_1(R)$ correspond to almost the same values of the equilibrium distance, that is, $R_0 \approx R_1$. In cases (b) and (c), $R_0 \neq R_1$. The horizontal lines in Figure 3. indicate schematically -and not to scale- the vibrational energy levels in the two electronic states. In all three figures, transitions will correspond to vertical lines according to the Franck-Condon principle (no change in r_{AB}). Furthermore, the vertical arrows start on the lower potential curve, and end on the upper potential curve. (Transitions can also occur which start from above the lower potential curve -indicating some kinetic energy- and end at a corresponding distance along the upper potential curve, but they are less likely as apart from the $v''=0$ level, the molecule spends most time where the oscillation amplitudes are their maximum, where the particles turn around.)

We shall assume that initially the molecule is in the electronic state $|0\rangle$, the nucleus performs zero-point oscillations around the equilibrium position R_0 , and the initial energy of the molecule is equal to $E_0(R_0)$, if we neglect the vibrational zero-point energy. If now light causes a transition to the electronic state $|1\rangle$, during the transition the nuclei will hardly change their position, and the molecule goes over into a state with energy $E_1(R_0)$. The energy involved in the transition will thus be equal to $\Delta U = E_1(R_0) - E_0(R_0)$. In case (a) the nuclei in the molecule perform zero-point oscillations both in the initial and in the final states. Such a transition can be called a pure electronic transition: $\Delta U = \Delta U_e$. In case (b) the molecule has gone after the

transition into a state $|1\rangle$ at $R=R_0$ which is not at the same equilibrium position R_1 of a state $|1\rangle$. The nuclei in the molecule will, therefore, in this state perform oscillations around the equilibrium position with an energy $G'(v')$ (equation (2)) where v' corresponds to the quantum number determining the excited vibrational state. In that case, the energy involved in the transition will be given by the equation $\Delta U = \Delta U_e + G'(v') - G''(0)$, where $\Delta U_e = E_1(R_1) - E_0(R_0)$.

In case (c) the quantum transition leads to a state corresponding to a continuous spectrum. When a transition to that state takes place, the nuclei of the molecule can move to infinite distances from one another corresponding to a photo-dissociation of the molecule.

Because of the zero-point oscillations of the nuclei in the initial state, the value $R=R_0$ is only the most probable one. Apart from the transitions indicated in Figure 3. by full-drawn arrows, there is also the possibility of less probable transitions accompanied by the excitation of other vibrational states, for instance, those indicated by dashed arrows. We see thus that it is possible that there is not just one transition, but a whole series of transitions corresponding to the excitation of various molecular vibrations. This gives rise to an electronic-vibrational band, which is still further complicated by the presence of rotational states. In the case shown in Figure 3. when the transition takes place to a state of the continuum, the band of excited states is continuous.

To obtain a quantitative picture of the intensity distribution of E1-transitions in the electronic spectrum, we must evaluate the

matrix elements,

$$\langle 2v' | r | 1v'' \rangle = \int \psi_2^*(r, R) \Phi_{v'}^*(R) r \psi_1(r, R) \Phi_{v''}(R) d r d R \quad (10)$$

of the electrical dipole transition with respect to the wave functions of the adiabatic approximation, which are products of the electronic wave functions $\psi(r, R)$, in which the nuclear coordinates R occur as parameters, and the wave functions $\Phi(R)$ describe the nuclear motion, and r is the electronic coordinate.

The matrix element

$$M_{21}(R) = \int \psi_2^*(r, R) r \psi_1(r, R) d r \quad (11)$$

is a slowly varying function of the nuclear coordinates R , since the electronic wave function depends only weakly on R for small displacements R from the equilibrium positions. We can thus expand M_{21} in a power series

$$M_{21}(R) = M_{21}(R_0) + \left[\frac{\partial M_{21}}{\partial R} \right]_{R=R_0} (R - R_0) + \dots \quad (12)$$

Substituting this value into $\langle 2v' | r | 1v'' \rangle$, we get

$$\langle 2v' | r | 1v'' \rangle = M_{21}(R_0) \int \Phi_{v'}^*(R) \Phi_{v''}(R) d R \quad (13)$$

where v' and v'' are the quantum numbers of the two vibrational levels of the upper and lower electronic states between which the transition takes place. The integral

$$\langle v' | v'' \rangle = \int \Phi_{v'}^*(R) \Phi_{v''}(R) dR \quad (14)$$

is called the overlap integral of the wave functions describing the nuclear motion. The absolute square of this quantity,

$$W_{v',v''} = |\langle v' | v'' \rangle|^2 \quad (15)$$

determines the relative intensity of the transition between the states v' and v'' , that is $w_{v',v''}$ characterizes the intensity distribution in the band, corresponding to the electronic transition $1 \rightarrow 2$. We have $\sum w_{v',v''} = 1$, that is, the total transition probability from one vibrational state of the initial state to all vibrational states of the final state depends only on the probability of the electronic transition which is proportional to $|M_{21}(R_0)|^2$. If we know that the overlap integral of the wave functions is non-zero for a particular v' and v'' , this means the transition is allowed between these two energy levels. From these two allowed energy levels, we can check the wavelength from our experimental results.

CHAPTER III

EXPERIMENT

To carry out measurements of the absorption cross-sections, it is necessary to confine a column of Na_2 vapor between transparent windows, through which a beam of light of given frequency is passed. For metal and metal-like elements, heat-pipe systems [15] [16] are well suited to generate the molecular vapor. Figure 4. shows a schematic of a heat-pipe and we shall first discuss operation in the "heat pipe mode".

In the heating zone the material is vaporized. The vapor streams to the cooling zones, where it condenses and becomes liquid and finally flows back within the metal mesh by capillary forces. A buffer gas is introduced as shown. The feed in has to be symmetrical at both ends and with sufficient power into the heating zone, the vapor pressure can be adjusted by the applied buffer gas pressure. The temperature T_p within the vapor zone will be obtained from the vapor pressure versus temperature curve (see Figure 5.). The buffer gas in the cooling zone and vapor in the vapor zone should be at the same pressure reading P , and a variation of the heating power changes the length of the vapor zone without changing T_p at constant buffer gas pressure. The main advantage of a heat-pipe is that aggressive metal vapors are kept away from the optical windows and the

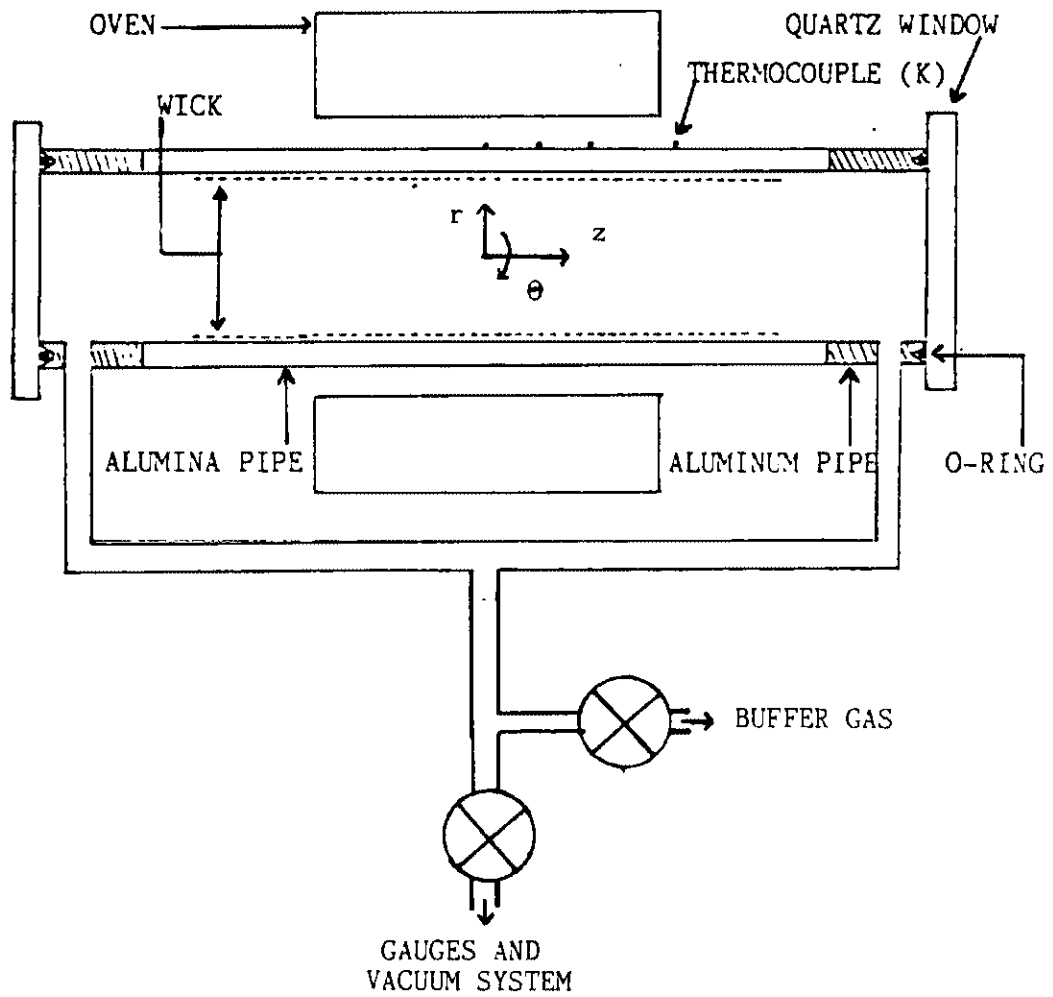


Figure 4. Heat-pipe used in experimental studies.

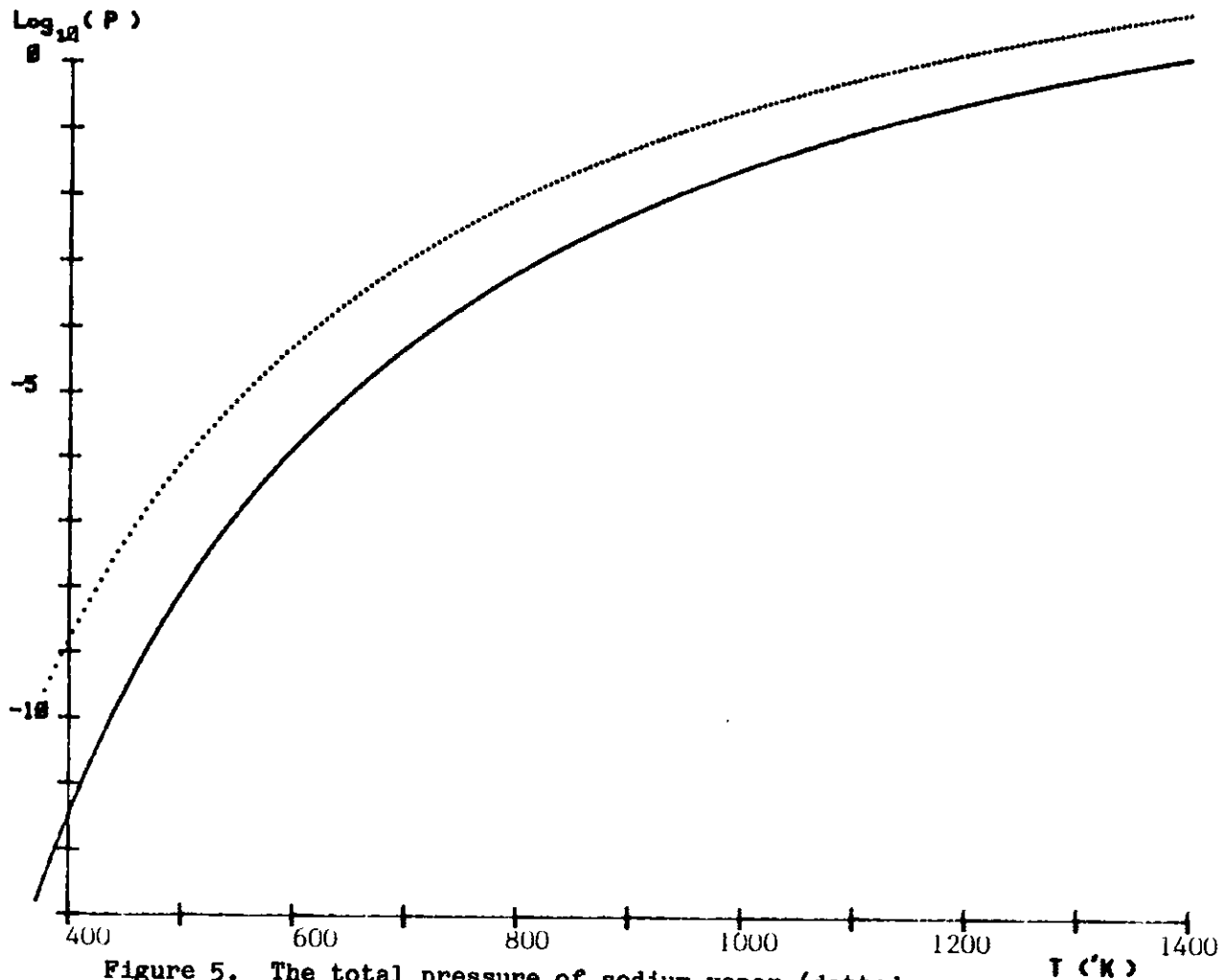


Figure 5. The total pressure of sodium vapor (dotted curve) and the partial pressure of sodium diatoms (solid curve) are functions of temperature. The experimental data is taken from reference [21].

parameters and the kind of buffer gas and pressure of buffer gas can be easily changed. The problem is that the length of the vapor zone; namely the length of optical path is difficult to estimate.

To operate a heat-pipe under ideal conditions, a sufficient amount of sodium is needed to wet the wick of the evaporator, which is inside the pipe, one-meter-long and 2.5 centimeter diameter. The needed amount is 50-80 grams sodium costing \$500-\$800. To save sodium (10 grams sodium in our case), we operated a non-heat-pipe mode which indicated the temperature T was smaller than T_p .

For $T < T_p$, which means the heat-pipe was operated under a "non-heat-pipe" mode, the $\text{Na}_2 + \text{Na}$ vapor pressure reading at the center is lower than P which is the reading of buffer gas pressure in the cool ends of the heat-pipe and which in turn is the total pressure inside the complete heat-pipe. In the vapor zone there is a mixture of the vapor with a partial pressure $P_p(T)$ and buffer gas with a partial pressure $P - P_p(T)$. In our case we estimated $T(r, z)$ as a function of position, which then gave $P_p(r, z)$ after the system was settled into a steady state. A monochromator scanned the light passing through the heat-pipe to obtain the absorbed spectra versus wavelength. We integrated the density of the sodium dimers of the pipe point by point, and used Beer's law to calculate the absorption cross-sections from those results.

1. Apparatus:

The system, shown diagrammatically and pictured (Figure 6a. & b.), functioned almost like a Cary-14 spectrophotometer. The Cary

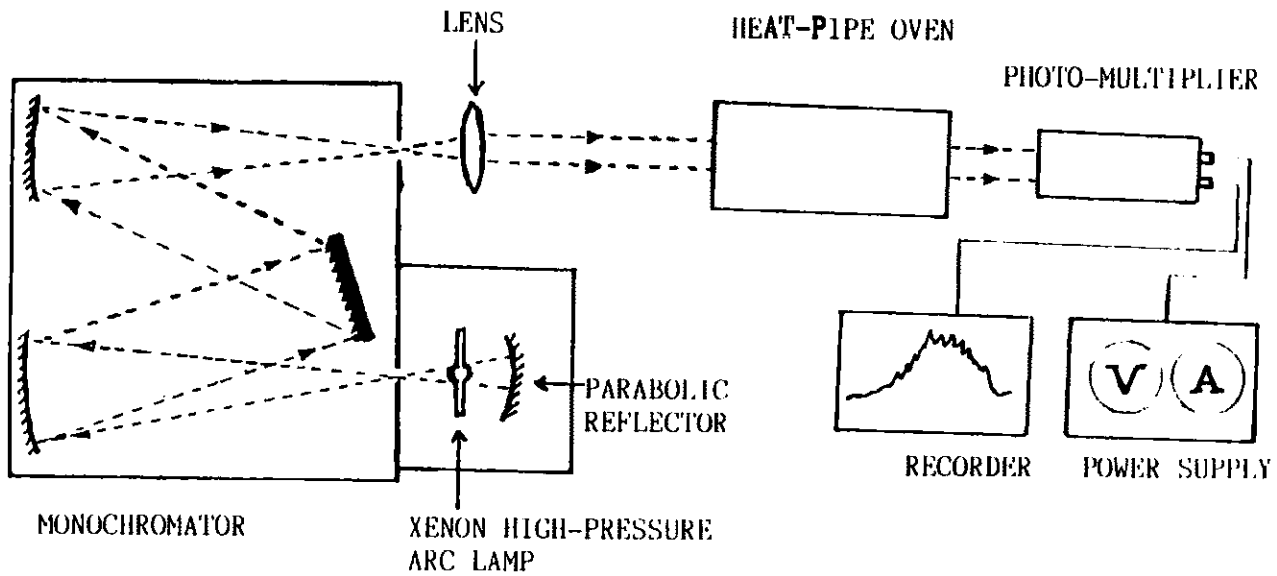


Figure 6a. Experimental arrangement designed to study the absorption cross-sections of sodium dimers.



Figure 6b. Experimental setup for measuring the absorption cross-sections of sodium dimers.

recording spectrophotometer model 14 is designed for automatic recording of absorption spectra in the wavelength region of 186nm-2,600nm with good resolving power and high photometric accuracy. Here, the heat-pipe was too big to be put into the sample cell of a Cary-14, so we had to build our own system. The light source was a 75 watt xenon high-pressure arc lamp with a parabolic reflector, focal length 12.7 cm, which focused on the entrance slit of the monochromator. A short arc power supply made by P.E.K. inc. series 401A with 20 volts and 10 amperes maximum output was the power source of the xenon arc lamp. The monochromator was a GCA/Mapherson instrument model 216.5, 0.5 meter scanning monochromator/spectrograph with a grating of 1200 lines per millimeter, used here as a narrow band filter, the center frequency of which could be changed by rotating the angle of the grating. The entrance and exit slits were set to 50 μm with the band width of the monochromator at about 0.85 \AA . For near ultraviolet spectra observation, a quartz lens of 5 cm focal length was put in front of the exit slit of the monochromator, which adjusted the output light to be parallel and to pass through the heat-pipe. The photo-multiplier detector, RCA 7264, with a type Na-K-Cs-Sb photocathode, was put on the far side of the heat-pipe. A high voltage regulated D. C. power supply made by Power Designs Pacific inc. model 3K-40 with 3,000 volts and 40 mA maximum output provided the operating voltage to the photo-multiplier tube. An X-Y recorder, Hewlett Packard 7046A, was used to plot the intensity of light versus wavelength.

The heat-pipe, shown in Figure 4., was constructed of 1-1/4 inch O.D. alumina pipe with a 1/8 inch thick wall 40 inches in

length. Inside the pipe was placed a wick constructed of 2-3 layers of 80 mesh stainless steel screen. The wick was used to move the liquid sodium back to the heated portion of the pipe by capillary action. Because of the fragility of the alumina pipe, we could not perform cutting operations directly on it. Accordingly two pieces of aluminum pipe about 3-1/2 inches long were added to both ends of the alumina pipe and joined by torr seal. On the outside ends of each of the added pipes a notch was cut for the purpose of positioning an O-ring. With the aid of O-rings, two quartz windows were attached to both ends of the heat pipe. Holes were drilled in the side of the aluminum pipes to connect with a copper tube to a Veeco vs-9 vacuum system in order to keep a constant and balanced pressure of buffer gas in each side.

The buffer gas for this case was helium supplied by Linde Co. with a purity 99.99%, whose purpose was to protect the quartz windows from coating by the sodium vapor. The same pressure at each side of the pipe kept the sodium vapor at center of the pipe and also made the temperature profile of the pipe symmetrical. A Wallace & Tiernan's pressure gauge, with a 200 torr full scale reading, monitored the pressure of the helium.

The heating element was a 12-1/2 inches long oven having a 6.7 ohm internal resistor from Marshall furnaces controls products. A variac controlled the input voltage to the oven, and a digital voltage meter indicated how much power was applied. The temperatures were monitored with 4 K-type thermocouples (alumel-chromel) which were calibrated by ice water and boiling water before starting the experiment. These thermocouples were placed in a row outside the

pipe with all of them in direct contact. Three of them were inside the oven at 2 inches separation starting from the center of the pipe. Only one thermocouple was outside the oven at a distance of 6-7/8 inches from the center of the pipe. A multiple switch selected one of them at a time to the Fluke 2190A digital thermometer.

2. Calibration:

Mercury light was used as one of the reference lamps. The mercury lamp was a pen ray lamp produced by the Ultraviolet Products company and was placed at the location of the xenon high pressure arc lamp. Scans were taken at the following wavelength ranges: 300nm-420nm, 430nm-550nm, and 560nm-680nm. The scan speed was non-uniform. The only needed calibration was the rotational speed of the grating of the monochromator to obtain a relation between the true wavelength and the position X of peaks in the spectrum on the chart. We initially recorded the mercury light spectrum [17] at the readings of the monochromator 3,000Å, 4,300Å and 5,600Å and then established the following three equations (see Appendix A).

$$\lambda = 0.0124065X^2 + 31.959235X + 3020.7489$$

$$\lambda = 0.0089886X^2 + 32.154454X + 4310.1209 \quad (16)$$

$$\lambda = 0.0967990X^2 + 30.829959X + 5607.2507$$

where X is the distance from starting point to measured point in the

recorded figures (see Figure 7., 8. and 9.) and is measured in centimeter.

3. Experimental process:

After we aligned and calibrated the system, we needed to bake the pipe at a high temperature around 500°C in vacuum in order to clean the pipe and also check the system did not have defects. 10 grams sodium would be used in our case of 99.95% purity, a product of the Alfa company. The sodium was contained in a glass-tube in argon gas. To place the sodium at the center of the heat-pipe the following steps were performed. First: put the sodium on a holder, break the sides of the tube, and place them at the center of the heat-pipe with helium flowing out to prevent air from getting into the pipe. Second: put back both end-windows of the heat-pipe, turn off the helium flow, pump the heat-pipe to vacuum, and heat the heat-pipe to 150°C in order to melt the sodium. Third: because of the adhesive force, with the liquid sodium still in the glass tube, we needed to insert a helium-pipe into the heat-pipe to blow sodium out of the glass tube. After having removed the glass and the holder, we filled in the required amount of helium and set the variac to sufficient power. The maximum temperature of the heat-pipe must be below 800°K , to avoid the fact that the photo-multiplier tube detected the black body radiation from the oven. On some runs a Corning colored filter, series number I-59, was used to filter out the infrared. After heating for eight hours, the temperature no longer changed. At this time, the heat-pipe oven was in a steady

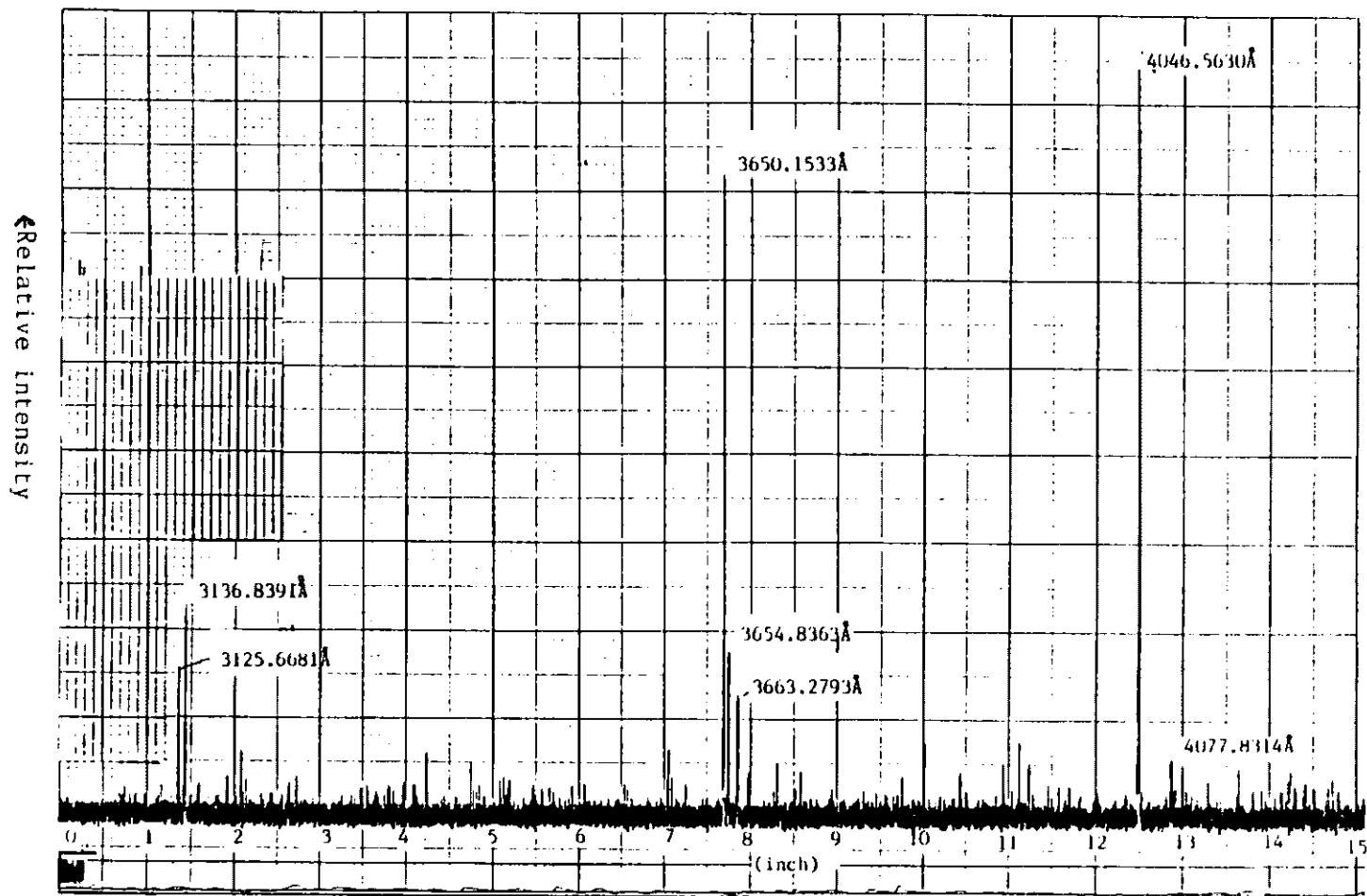


Figure 7. Mercury light spectrum from 300 nm to 420 nm (for calibration use).

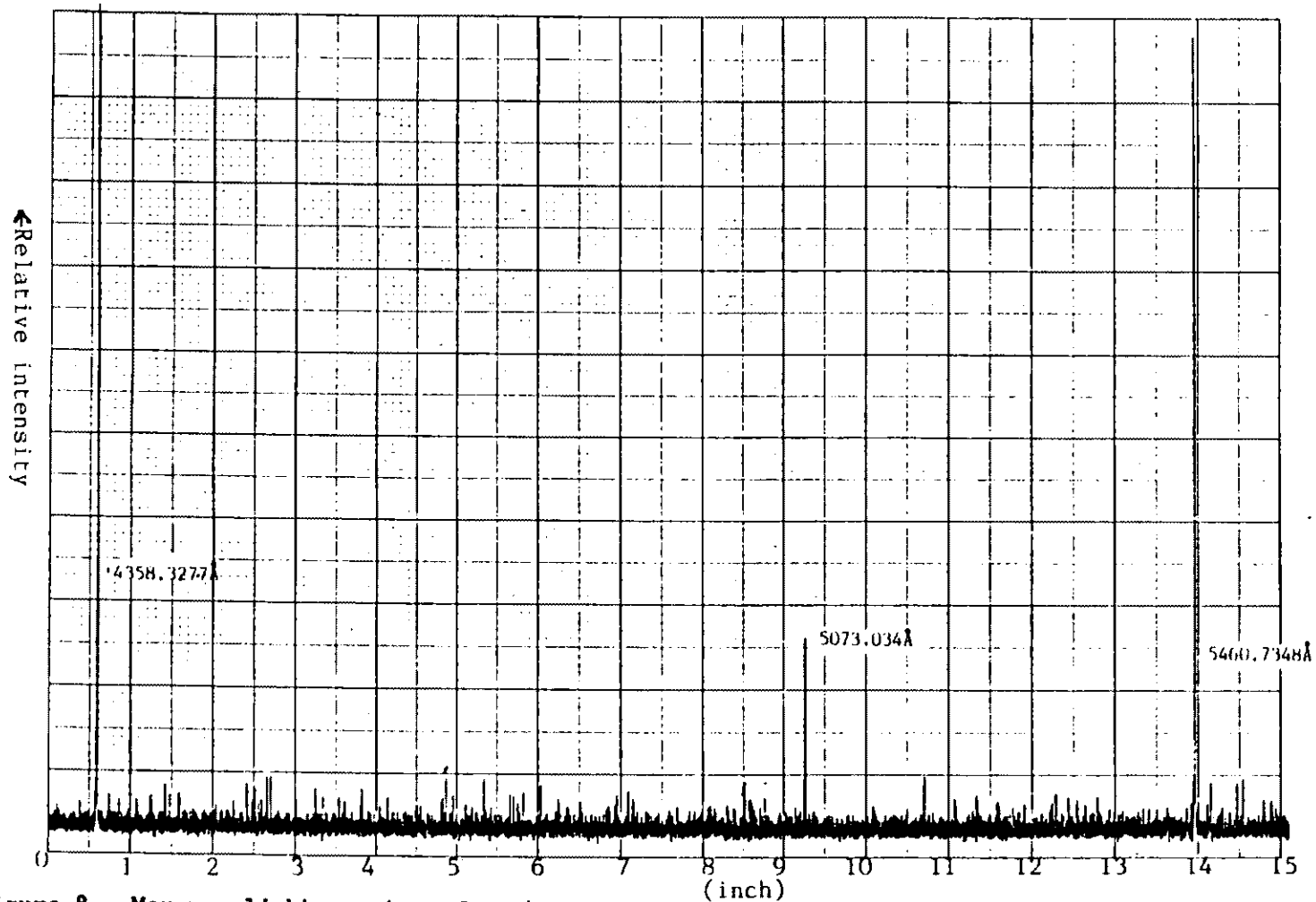


Figure 8. Mercury light spectrum from 430 nm to 550 nm (for calibration use).

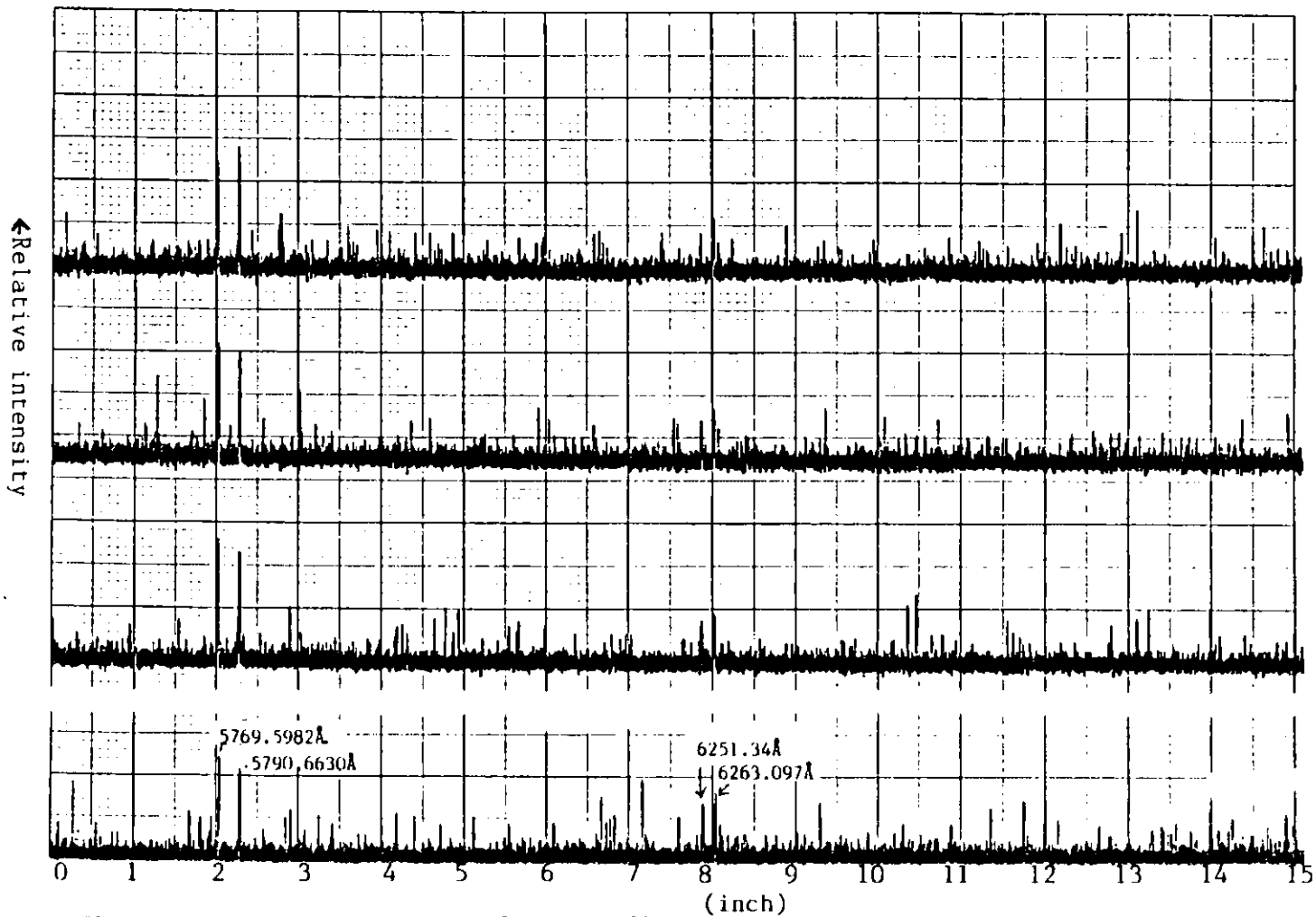


Figure 9. Mercury light spectrum from 560 nm to 680 nm and scan 4 times (for calibration use).

state but not in the heat-pipe mode. The xenon high pressure arc lamp was turned on and three time scans at the wavelength ranges were taken. The same process was then repeated at different temperatures.

After the temperature of the oven returned to the room temperature, we changed the pressure of buffer gas. Sodium was solid at room temperature and was not lost while we were using the vacuum system. Measurements were then made of the absorption versus wavelength for different pressures as well as temperatures.

CHAPTER IV

THE CALCULATION OF THE ABSORPTION CROSS-SECTIONS

Figure 10. to Figure 20. show intensity of light transmitted through the pipe versus wavelength, at different temperatures and at different buffer gas pressures. Comparing them with the background figures which recorded the intensity of light of the xeon-lamp passing through the heat-pipe under very low sodium vapor pressure (with temperature around 200°C inside the center of the heat-pipe), we found some wavelengths were reduced in intensity. According to Beer's law [18], if the intensity of a collimated beam of monochromatic light decreases from I_0^λ to I_t^λ over a path length L -cm and the concentration of the absorbing material is N -number of particles per cubic centimeter, then the absorption cross-section $\sigma(\lambda)$ is defined by

$$I_t^\lambda = I_0^\lambda \exp(-(\sigma(\lambda)NL)) \quad (17)$$

The value of $\sigma(\lambda)$ which is a function of wavelengths is then found to be

$$\sigma(\lambda) = \ln I_0^\lambda / I_t^\lambda / (NL) \dots \text{cm}^2 \quad (18)$$

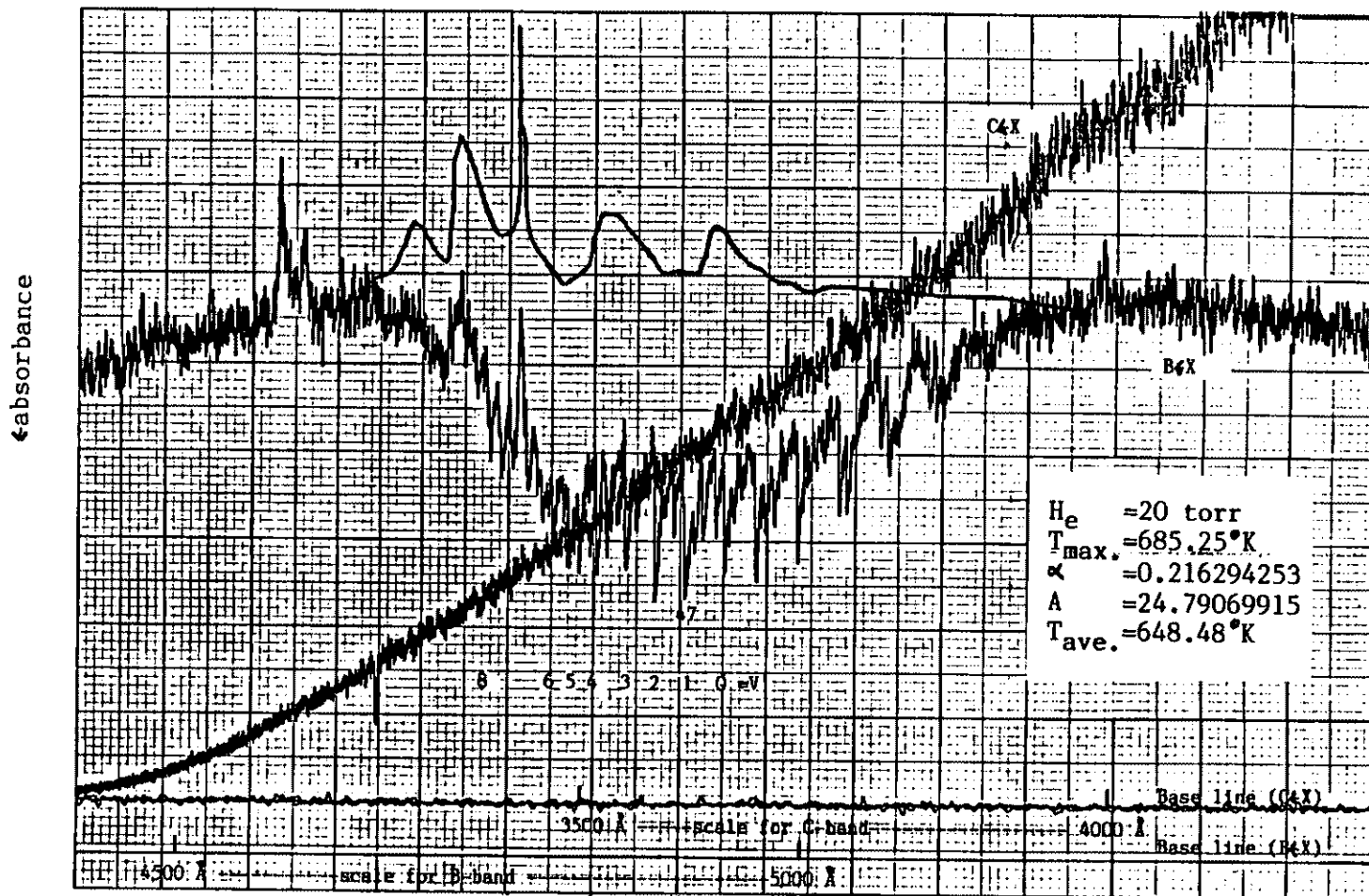


Figure 10. Two absorption spectra taken under helium pressure 20 torr and input power 162 watts for 2 different wavelength ranges (B \leftarrow X & C \leftarrow X transitions). \bar{n} (average sodium dimer density) \times L (optical path) = $8.713E+14$. The hand drawn curve for B \leftarrow X is the background (I_0). The actual signal had noise superimposed on the hand drawn curve. The absorption is proportional to the difference between the signal and I_0 . The C \leftarrow X curve is I_0 because the absorption of C-band was undetectable in this temperature.

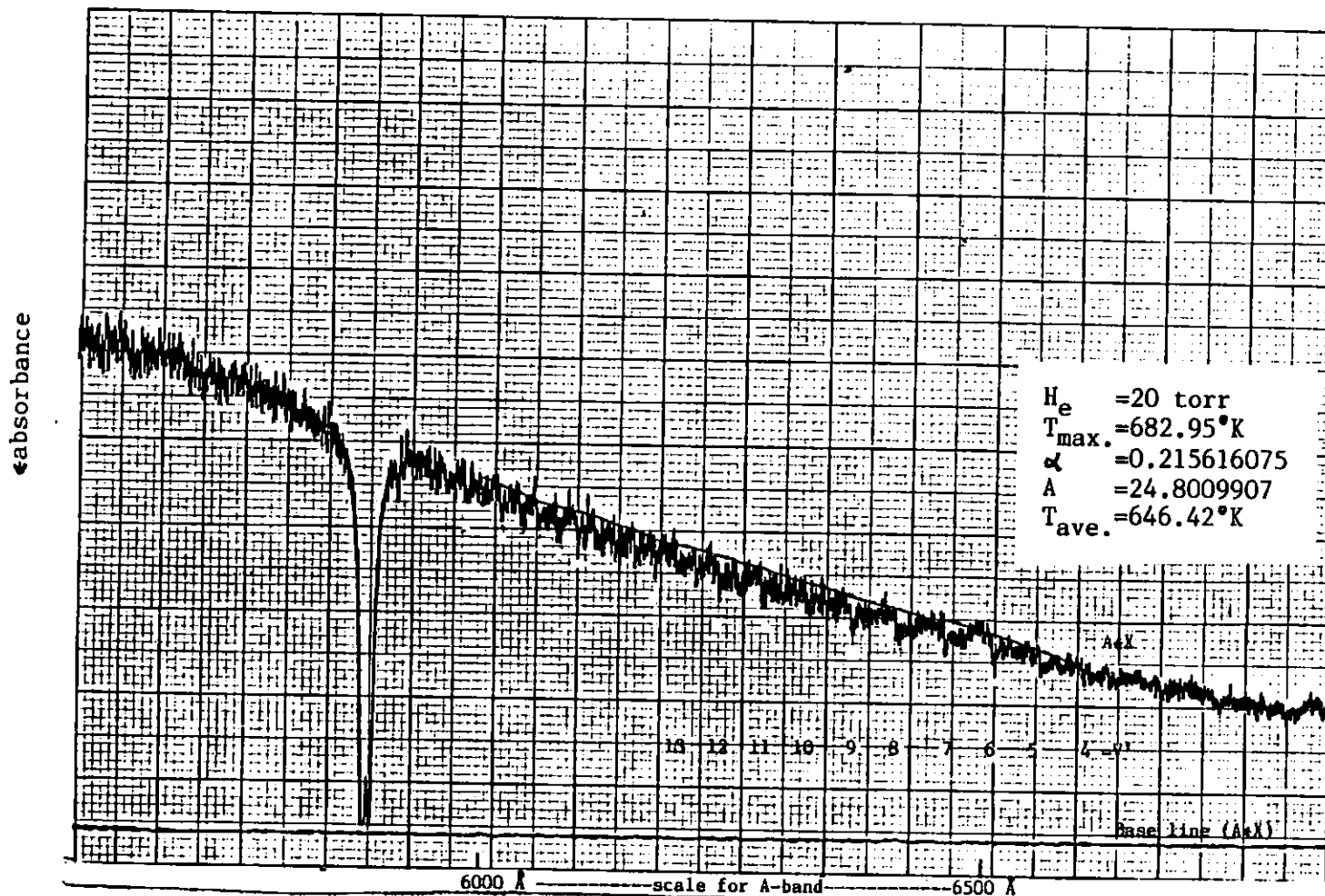


Figure 11. The absorption spectrum taken under helium pressure 20 torr and input power 162.5 watts for A \leftarrow X transitions. \bar{n} (average sodium dimer density) \times L (optical path) = $8.133\text{E}+14$. The hand drawn curve for A \leftarrow X is the background (I_0). The actual signal had noise superimposed on the hand drawn curve. The absorption is proportional to the difference between the signal and I_0 .

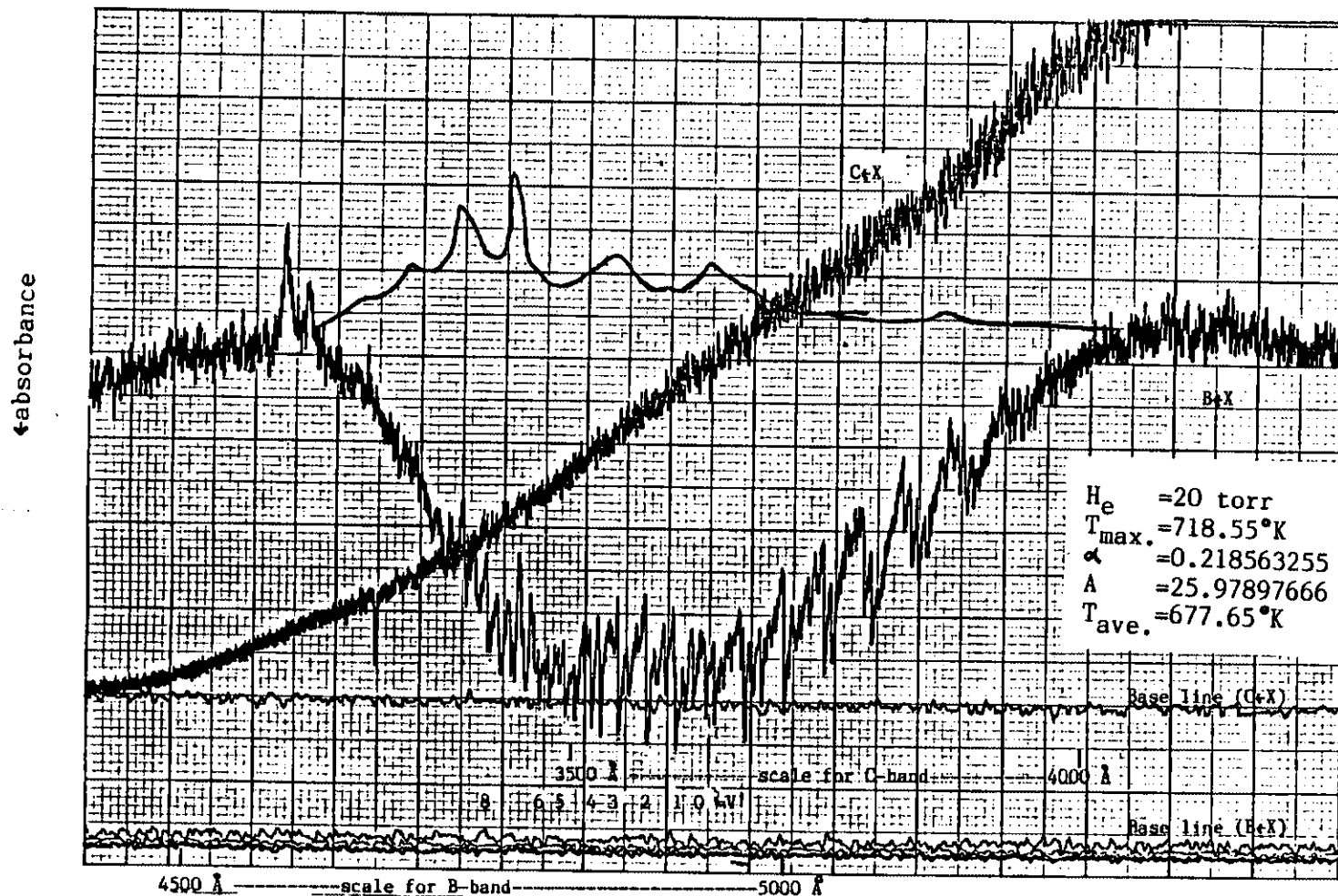


Figure 12. Two absorption spectra taken under helium pressure 20 torr and input power 192 watts for 2 different wavelength ranges (B←X & C←X transitions). \bar{n} (average sodium dimer density) x L (optical path) = $2.24E+15$. The hand drawn curve for B←X is the background (I_0). The actual signal had noise superimposed on the hand drawn curve. The absorption is proportional to the difference between the signal and I_0 . The C←X curve is I_0 because the absorption of C-band was undetectable in this temperature.

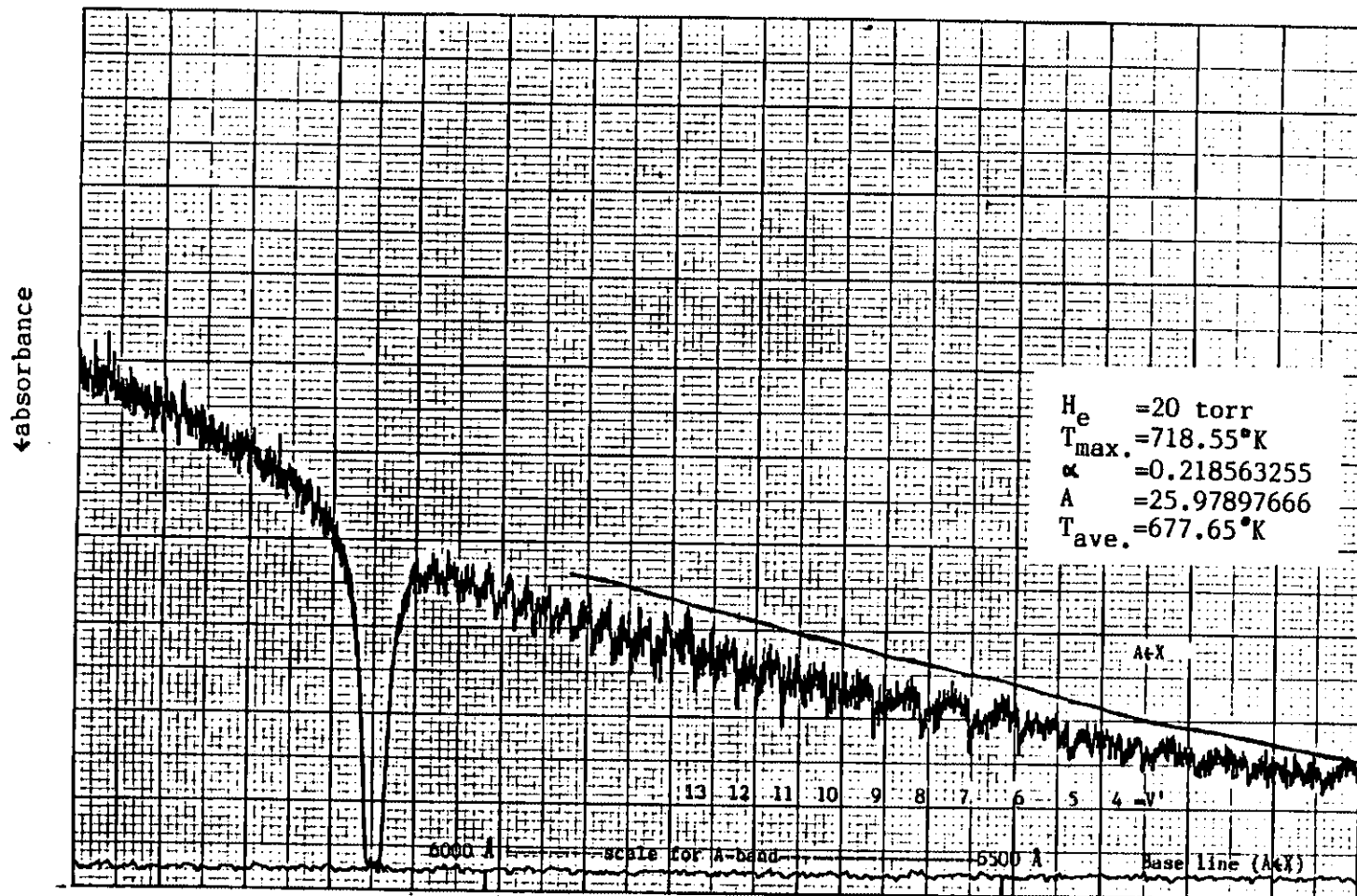


Figure 13. The absorption spectrum taken under helium pressure 20 torr and input power 192 watts for $A \leftarrow X$ transitions. \bar{n} (average sodium dimer density) \times L (optical path) = $2.24E+15$. The hand drawn curve for $A \leftarrow X$ is the background (I_0). The actual signal had noise superimposed on the hand drawn curve. The absorption is proportional to the difference between the signal and I_0 .

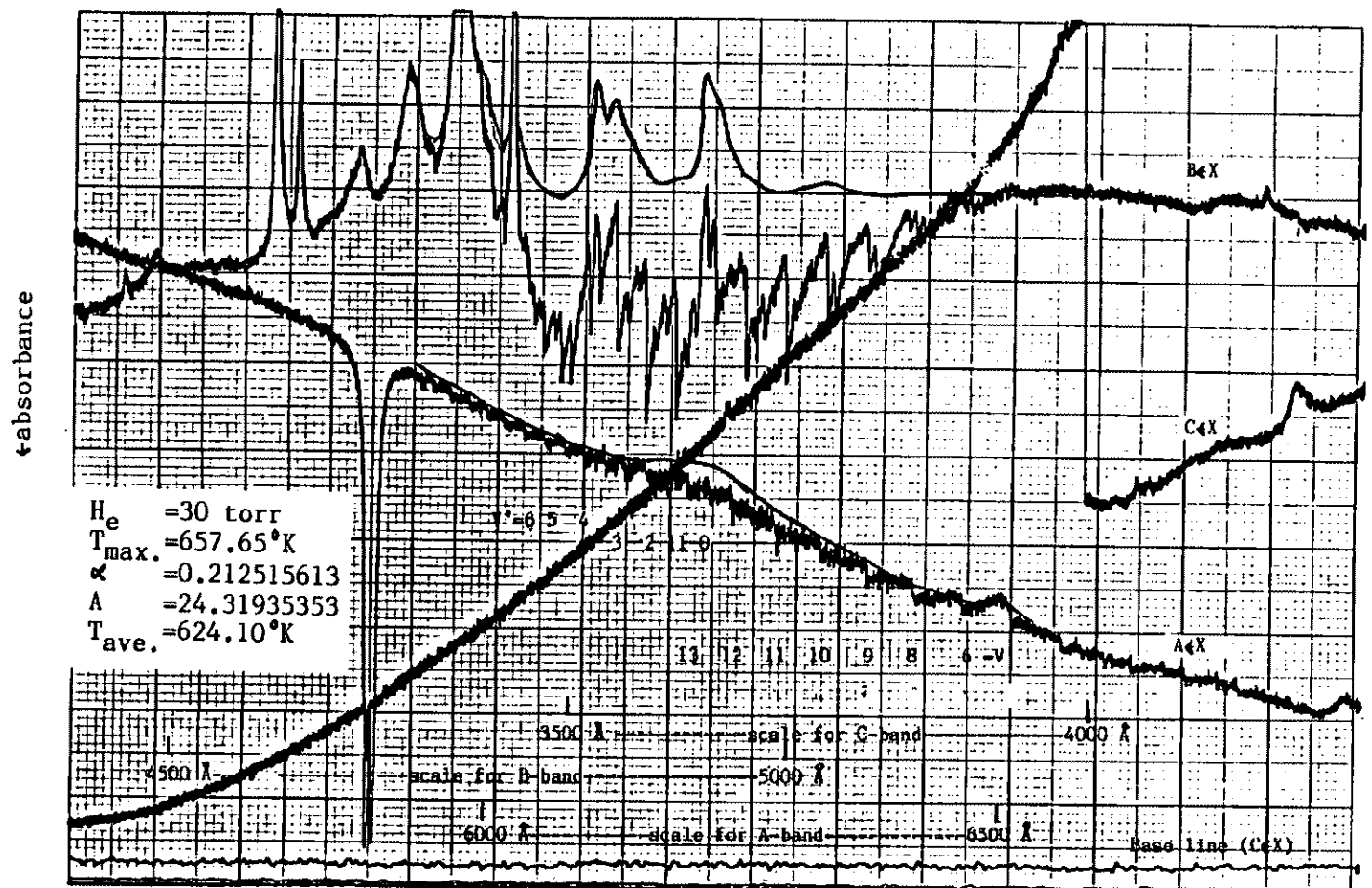


Figure 14. Three absorption spectra taken under helium pressure 30 torr and input power 152.5 watts for 3 different wavelength ranges (B\leftarrowX, C\leftarrowX & A\leftarrowX transitions). \bar{n} (average sodium dimer density) x L (optical path) = $3.65E+14$. The hand drawn curves for B\leftarrowX & A\leftarrowX are the background (I_0). The actual signal had noise superimposed on the hand drawn curve. The absorptions are proportional to the difference between the signal and I_0 . The C\leftarrowX curve is I_0 because the absorption of C-band was undetectable in this temperature.

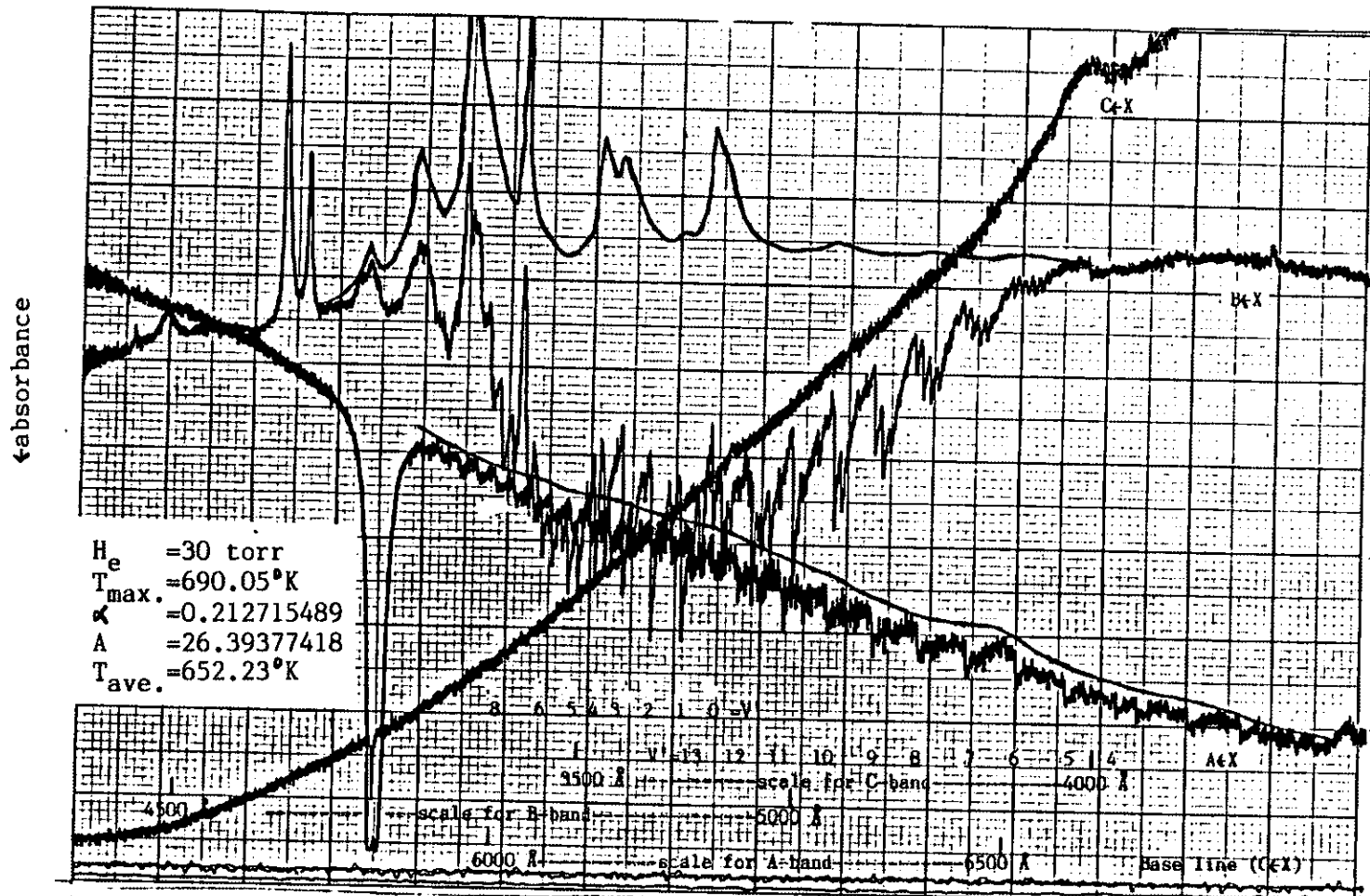


Figure 15. Three absorption spectra taken under helium pressure 30 torr and input power 165 watts for 3 different wavelength ranges (B-X, C-X & A-X transitions). \bar{n} (average sodium dimer density) x L (optical path) = $9.87E+14$. The hand drawn curves for B-X & A-X are the background (I_0). The actual signal had noise superimposed on the hand drawn curve. The absorptions are proportional to the difference between the signal and I_0 . The C-X curve is I_0 because the absorption of C-band was undetectable in this temperature.

← absorbance

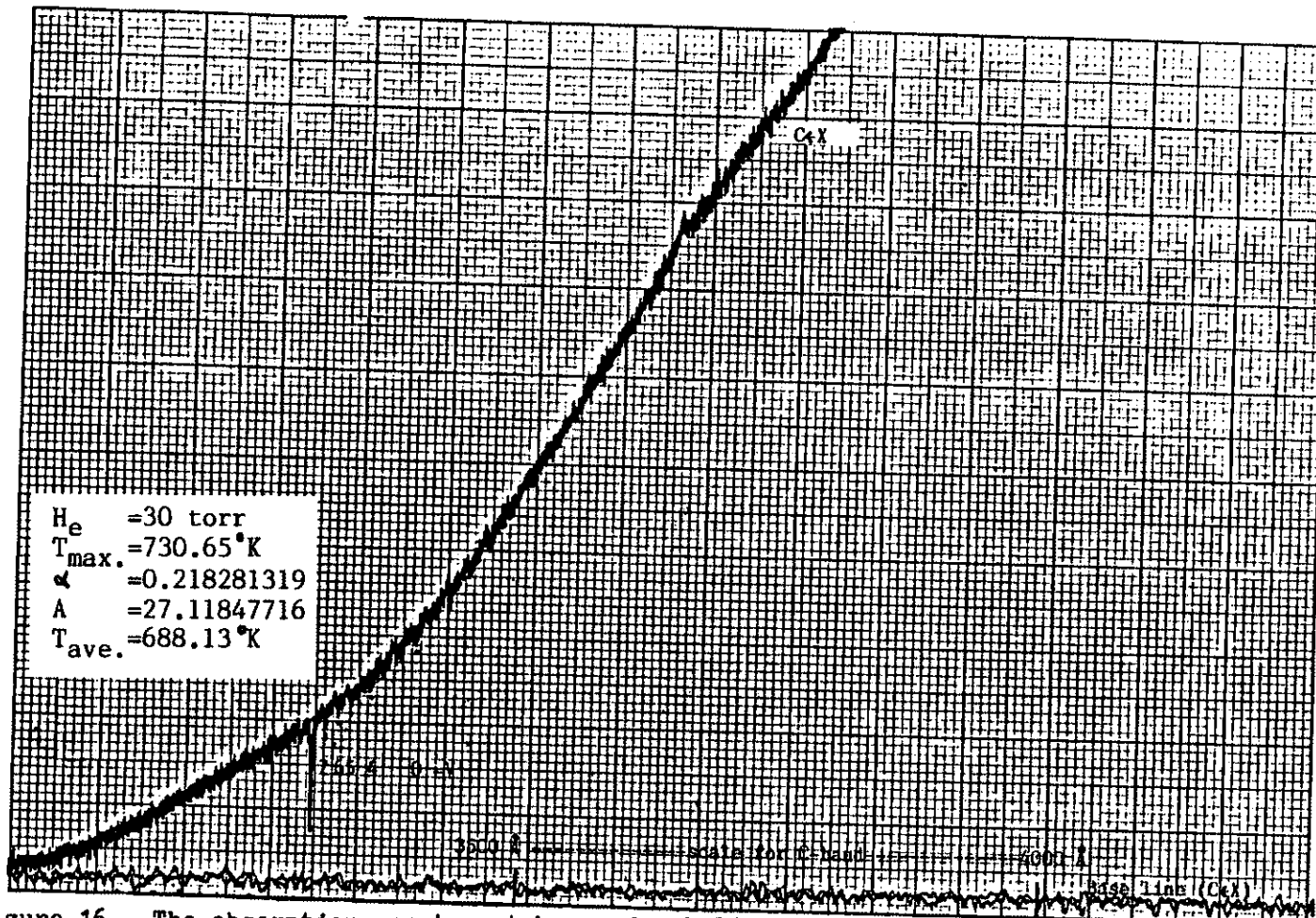


Figure 16. The absorption spectrum taken under helium pressure 30 torr and input power 185 watts for C-X transitions. \bar{n} (average sodium dimer density) x L (optical path) = 3.05E+15. The hand drawn curve for C-X is the background (I_0). The actual signal had noise superimposed on the hand drawn curve. The absorption is proportional to the difference between the signal and I_0 .

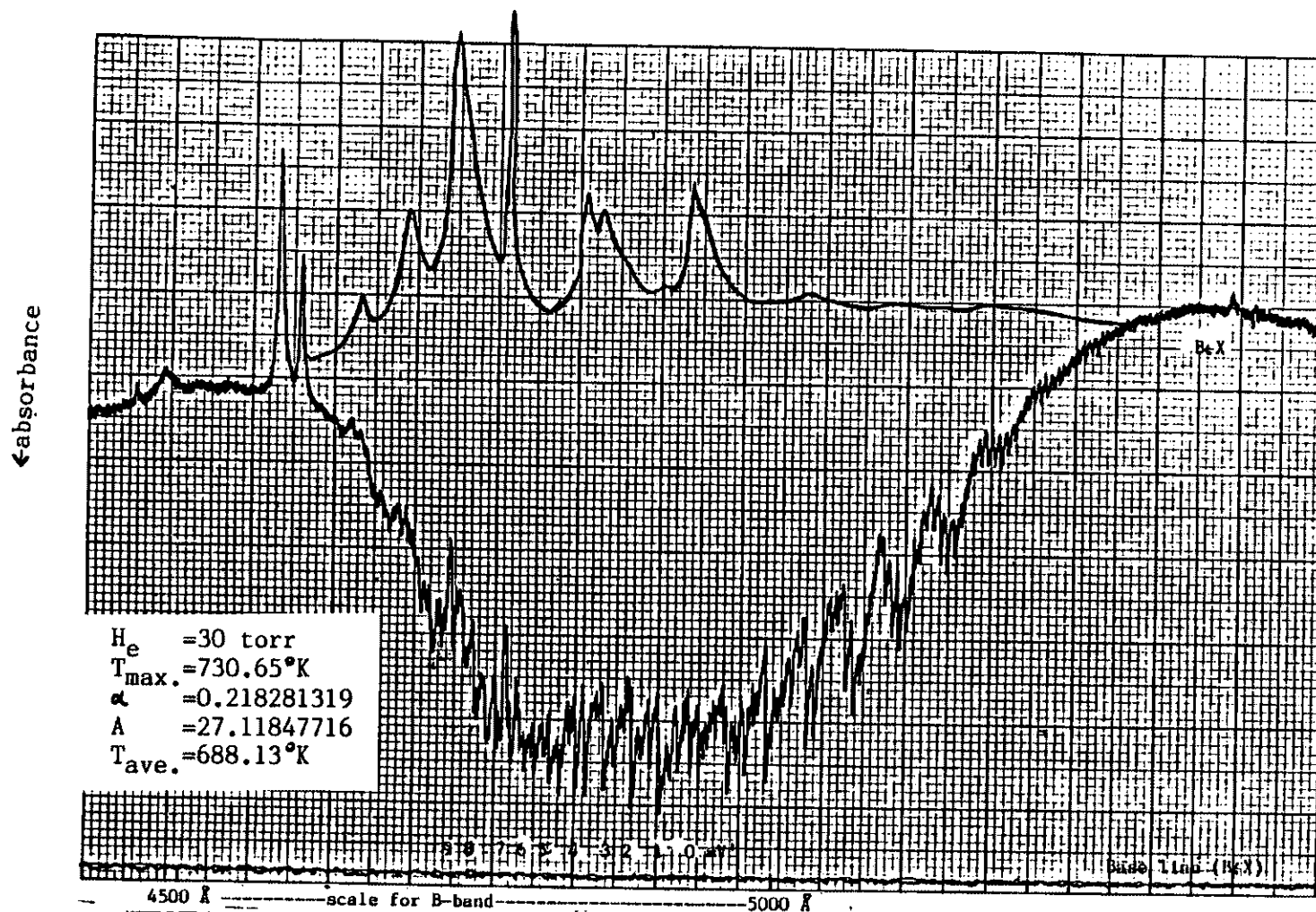


Figure 17. The absorption spectrum taken under helium pressure 30 torr and input power 185 watts for B-X transitions. \bar{n} (average sodium dimer density) \times L (optical path) = $3.05\text{E}+15$. The hand drawn curve for B-X is the background (I_0). The actual signal had noise superimposed on the hand drawn curve. The absorption is proportional to the difference between the signal and I_0 .

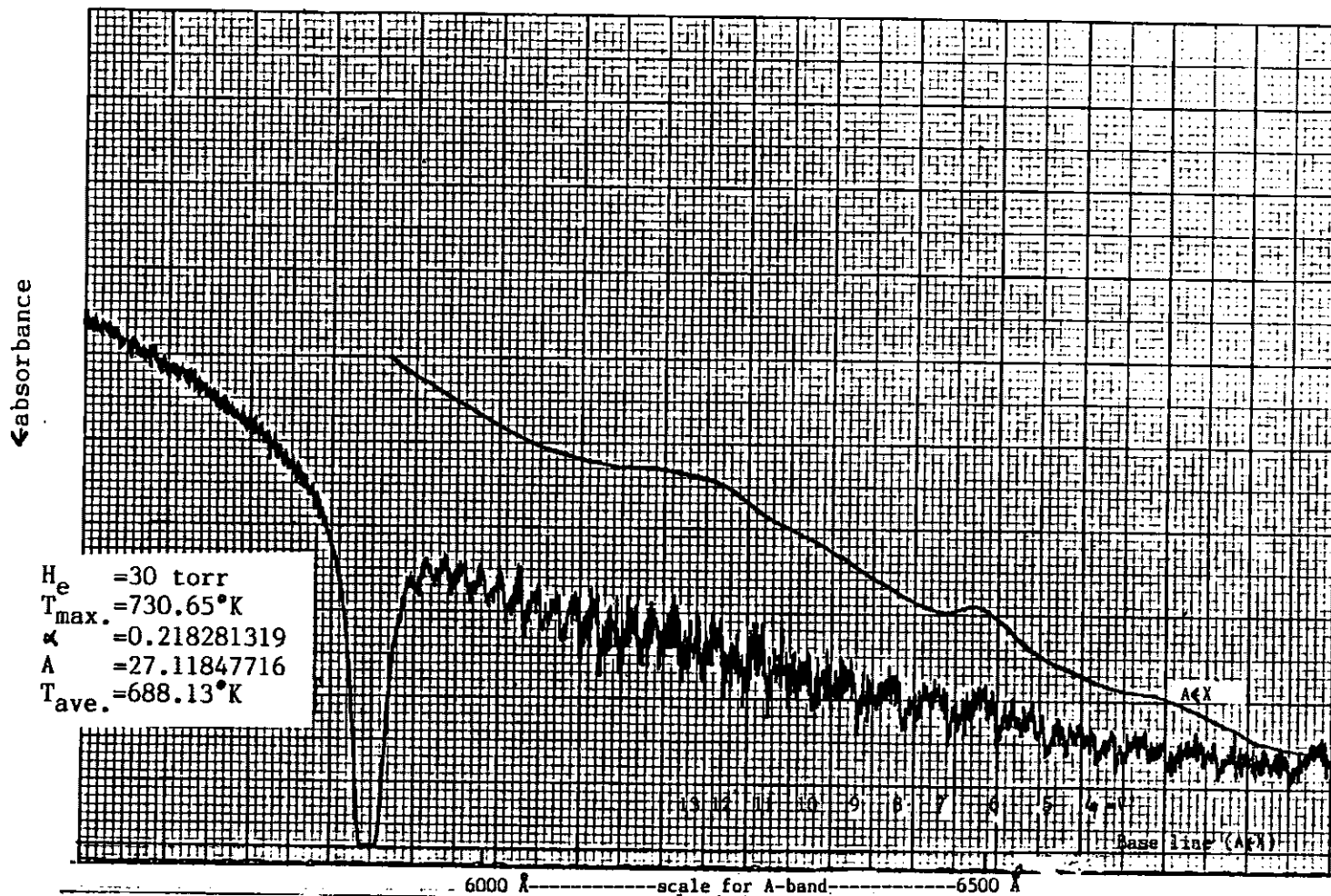


Figure 18. The absorption spectrum taken under helium pressure 30 torr and input power 185 watts for A \leftarrow X transitions. \bar{n} (average sodium dimer density) x L (optical path) = $3.05E+15$. The hand drawn curve for A \leftarrow X is the background (I_0). The actual signal had noise superimposed on the hand drawn curve. The absorption is proportional to the difference between the signal and I_0 .

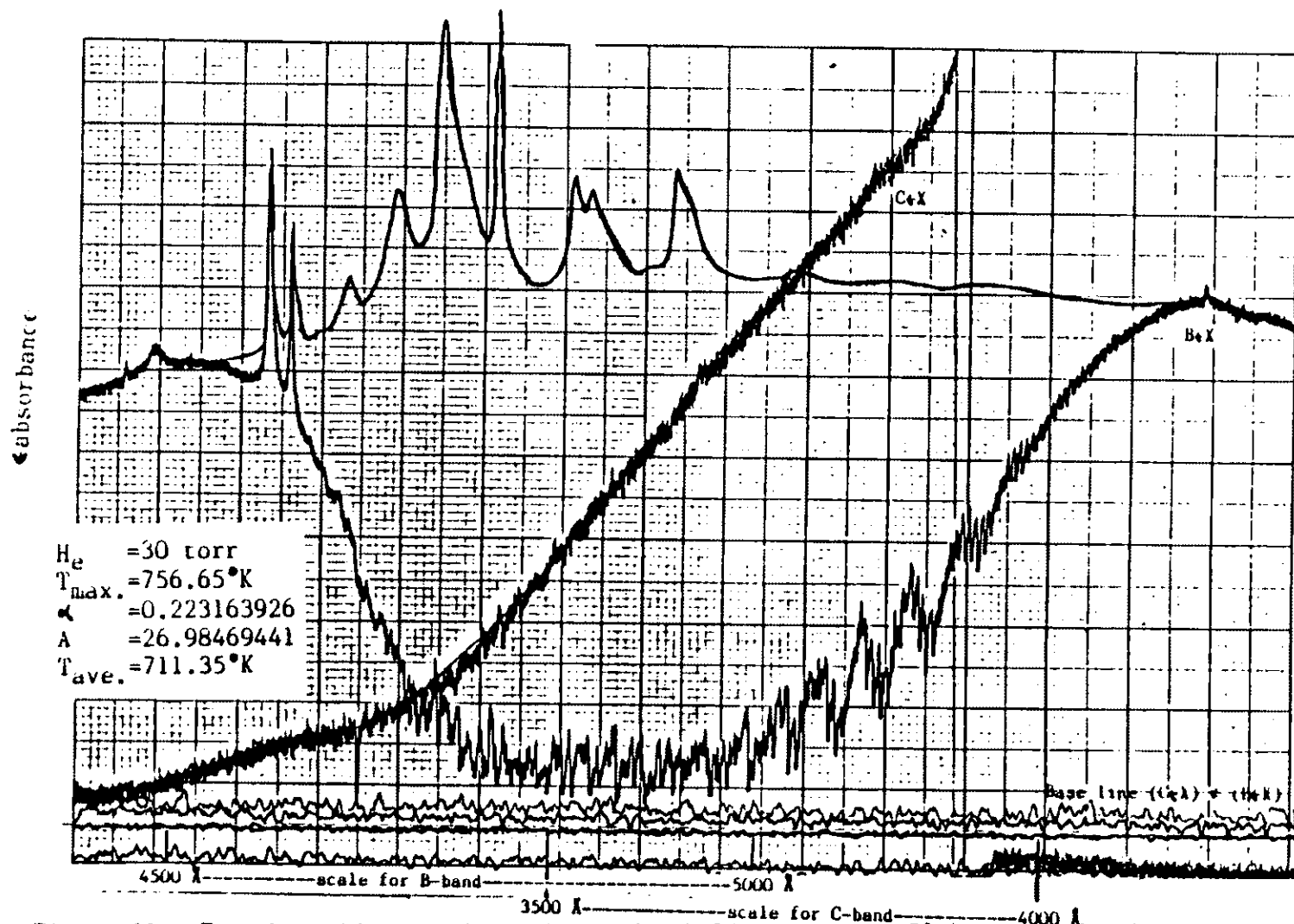


Figure 19. Two absorption spectra taken under helium pressure 30 torr and input power 207 watts for 2 different wavelength ranges (B \leftarrow X & C \leftarrow X transitions). \bar{n} (average sodium dimer density) x L (optical path) = $5.88E+15$. The hand drawn curves for B \leftarrow X & C \leftarrow X are the background (I_0). The actual signal had noise superimposed on the hand drawn curve. The absorption is proportional to the difference between the signal and I_0 .

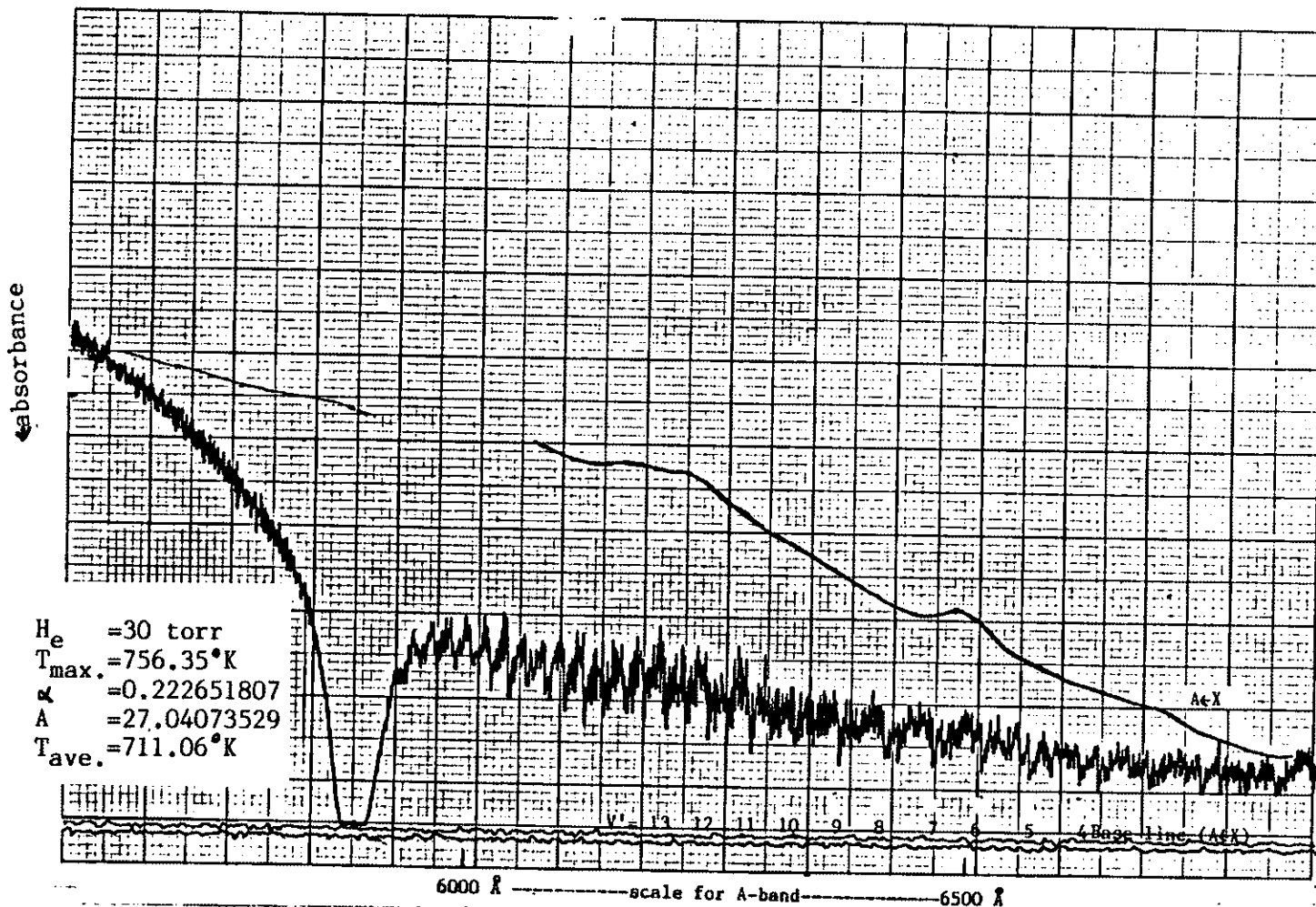


Figure 20. The absorption spectrum taken under helium pressure 30 torr and input power 212 watts for A \leftarrow X transitions. \bar{n} (average sodium dimer density) \times L (optical path) = $5.88E+15$. The hand drawn curve for A \leftarrow X is the background (I_0). The actual signal had noise superimposed on the hand drawn curve. The absorption is proportional to the difference between the signal and I_0 .

Sodium metal has a very low vapor pressure compared with other liquid heat transfer media, even at temperatures as high as 500°C (932°F) the vapor pressure is only 3 torr. If we know the pressure-temperature relation, the vapor density can be obtained from sodium vapor pressure by employing the ideal gas law.

The complete temperature dependence of vapor pressure requires a formula with four adjustable parameters. Many formulas have been suggested but the one found most satisfactory by Nesemeyanoy [19] is $\log_{10} P = A - B/T + CT + D \log T$. The four adjustable parameters were obtained from Sittig's book [20], and the total pressure of atomic sodium vapor is

$$\log_{10} P_{\text{total}} = 4.57791 - 5249.1/(T - 8.14) \dots \text{atm} \quad (19)$$

C and D are zeros. "8.14" is an adjusted value for reducing error. Equation 19 is valid for 400°K < T < 950°K.

The partial pressure of sodium diatoms is

$$\log_{10} P_{\text{Na}_2} = 4.340 - 5682/(T - 43) \dots \text{atm} \quad (20)$$

C and D are again zeros, and "43" is an adjusted value for reducing error. The range of validity is 500°K to 1025°K.

We estimated the maximum error by comparing equation (20) with the experimental data indicated in Sittig's book, table A-9 [21]. The error percentage formula is theoretical value (equation (20)) minus experimental values, divided by the experimental value, and times 100. In the temperature range from 500°K to 800°K, the

error is less than 5% (see Figure 21.).

Since our heat-pipe was operated in the non-heat-pipe mode as mentioned in chapter III, we needed to know the temperature distribution versus position inside the heat-pipe (see Figure 22.). Unfortunately, it was difficult to measure the temperature inside the tube directly. The reason was that the sodium vapor would condense on the thermocouple causing the reading to be incorrect. However a simple theoretical derivation of the temperature distribution inside the tube was obtained. In the steady state, the input power must be equal to the output power. This means that the divergent energy flux must be equal to zero.

$$\vec{\nabla} \cdot \vec{q} = 0 \quad (21)$$

In cylindrical coordinates (r, θ, z) , there are three energy flux components inside the oven. They are

$$q_r = K \frac{\partial T}{\partial r}, \quad q_\theta = K/r \frac{\partial T}{\partial \theta}, \quad q_z = K \frac{\partial T}{\partial z} \quad (22)$$

where K is the thermal conductivity of gases inside the heat-pipe.

A single gas has a coefficient of heat conduction. $K = (\lambda^* c^* n^* C_v)/3$ where λ^* is the mean free path, c^* the random velocity, n^* the gas density, and C_v the specific heat of the gas at constant volume. The conduction is independent of the pressure ($\lambda^* n^* = \text{constant}$) and $\sim T^{1/2}$. The conduction mechanism is a transport of the hot particles with a diffusion coefficient $c^* \lambda^*/3$; hence, for a mixture of gases 1, 2 and 3, where 1=He,

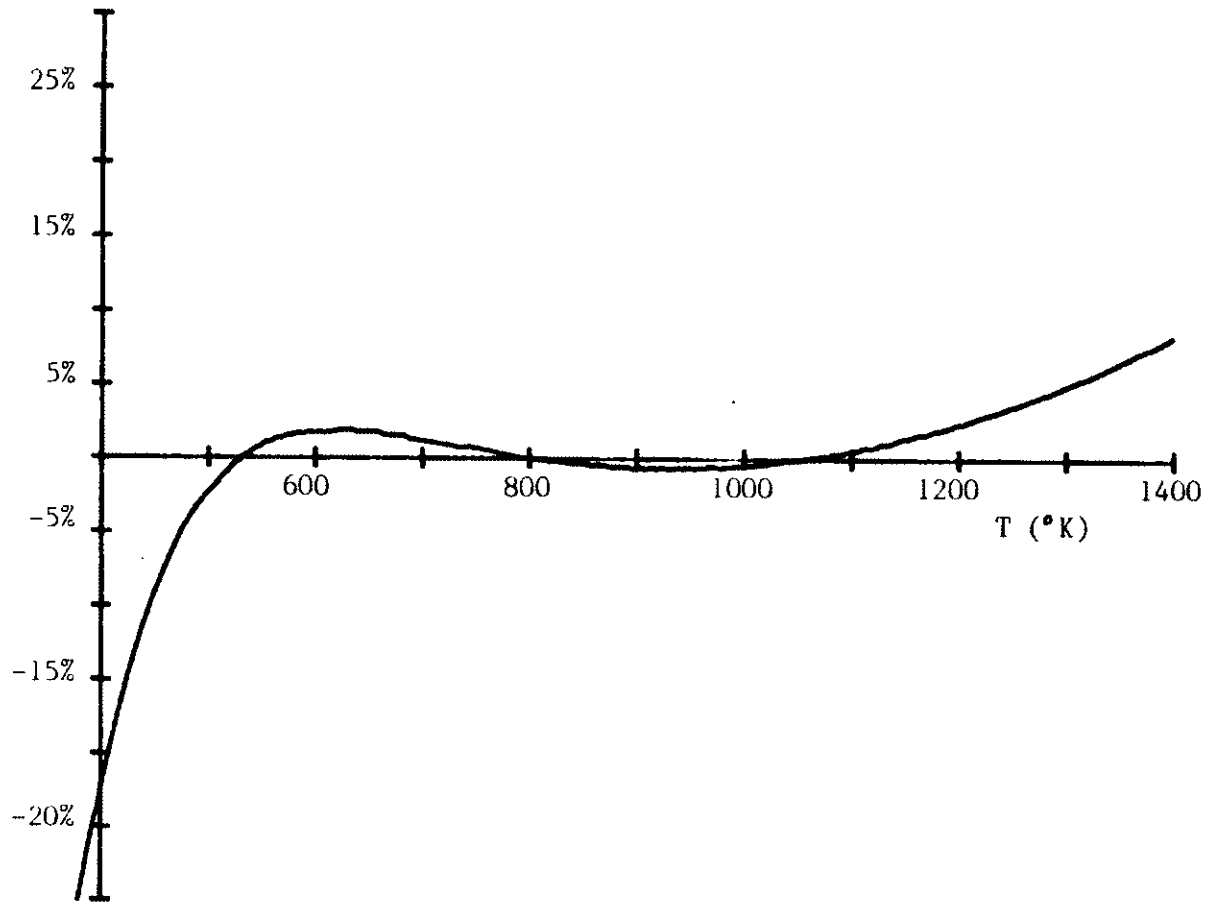


Figure 21. The error percentage of equation (20) versus temperature.

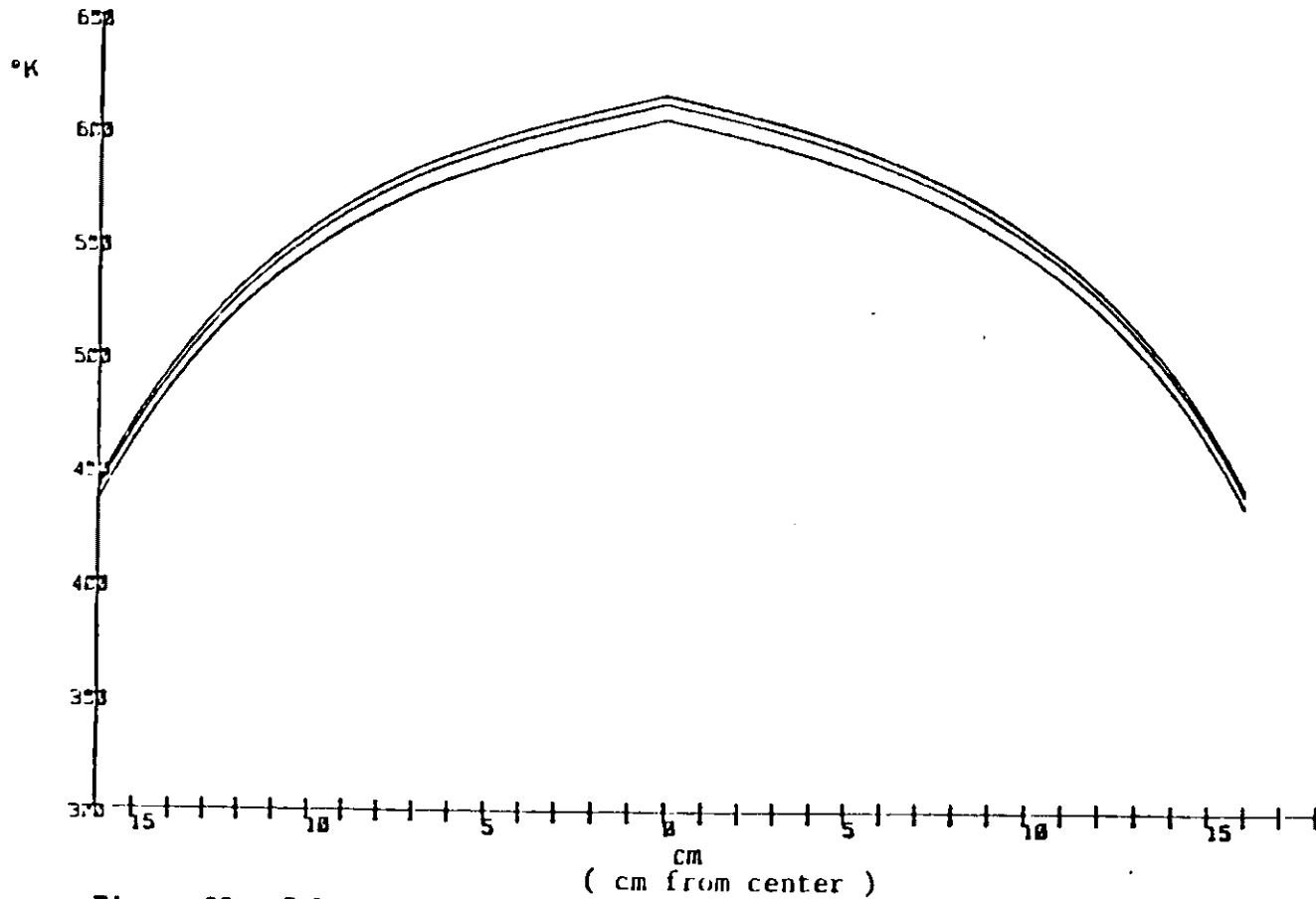


Figure 22. Calculated temperature profiles for the heat- pipe at helium pressure of 20 torr and 125 watts, input power. For $r=1.27\text{cm}$, $r=0.5\text{cm}$, and $r=0\text{cm}$ (r is semidiameter), we get three curves, the upper, the middle, and the lower.

2=Na, and 3=Na₂, the resultant coefficient K is [5]

$$K=K_{He}S(T/273)^{1/2} \quad (23)$$

and S is defined as follows:

$$S = \frac{1 + a \sqrt{\frac{m_2}{m_1}} \frac{C_{v,2}}{C_{v,1}} + b \sqrt{\frac{m_3}{m_1}} \frac{C_{v,3}}{C_{v,1}}}{1 + a \frac{\sigma_2}{\sigma_1} + b \frac{\sigma_3}{\sigma_1}} \quad (24)$$

where m_n = is molecular weight, $C_{v,n}$ = specific heat at constant volume, σ_n = collision cross-section. The coefficient is in terms of K_{He} as He has the highest conductivity.

Then the equation of the energy flux is

$$\frac{1}{r} \left\{ \frac{\partial}{\partial r} \left(\frac{k_{He} S \sqrt{T}}{\sqrt{273}} r \frac{\partial T}{\partial r} \right) + \frac{\partial}{\partial \theta} \left(\frac{k_{He} S \sqrt{T}}{\sqrt{273}} \frac{\partial T}{\partial \theta} \right) + \frac{\partial}{\partial z} \left(\frac{k_{He} S \sqrt{T}}{\sqrt{273}} r \frac{\partial T}{\partial z} \right) \right\} = 0 \quad (25)$$

To simplify equation (25), we consider the symmetry versus angle θ and separate the variables r and z .

$$T=T(r,z)=T_r T_z \quad (26)$$

We obtain two differential equations.

$$T_r'' + T_r' / r + (T_r'^2 / 2T_r^2 + \alpha^2) T_r = 0 \quad (27)$$

$$T_z'' + (T_z'^2 / 2T_z^2 - \alpha^2) T_z = 0 \quad (28)$$

where α is the separation constant.

This leads to (see Appendix B)

$$T_r = J_0^{2/3} [\sqrt{3/2} \alpha (1.27 - r)] \quad (29)$$

$$T_z = T_{\max} - A \sinh(\sqrt{2/3} \alpha z) \quad (30)$$

where J_0 is Bessel's function of the first kind and of index zero, T_{\max} , α , and A are three constants which match the boundary conditions of four measured temperature points on the wall of the pipe (see Appendix C).

Equations (29) and (30) give values of temperature T versus r and z , which in turn determine the partial pressure of Na_2 versus position. The total pressure will of course be constant.

According to the Maxwell-Boltzmann distribution law, the number of molecules dN_e that have a classical vibrational energy between E and $E+dE$ is proportional to $e^{-(E/kT)} dE$, where k is Boltzmann's constant and T is the absolute temperature. The function $e^{-(E/kT)}$ [$e^{-(E/0.6952T)}$, where E is expressed in cm^{-1}] is represented graphically in Figure 23. for Na_2 $T=500^\circ\text{K}$.

Classically there is no restriction for the E values (see Figure 23.). However according to quantum theory, only discrete values are possible for the energies of the vibrational states. The number of molecules in each of the vibrational states is again proportional to the Boltzmann factor $\exp[-(E/kT)] = \exp\{-[G(v)-G(0)]hc/0.6952T\} = \exp\{-(G_0(v)hc/0.6952T)\}$, where $G(v)$ is the energy in the vibrational level v and is calculated by using equation (2), and $G_0(v)$ is the energy gap between the vibrational

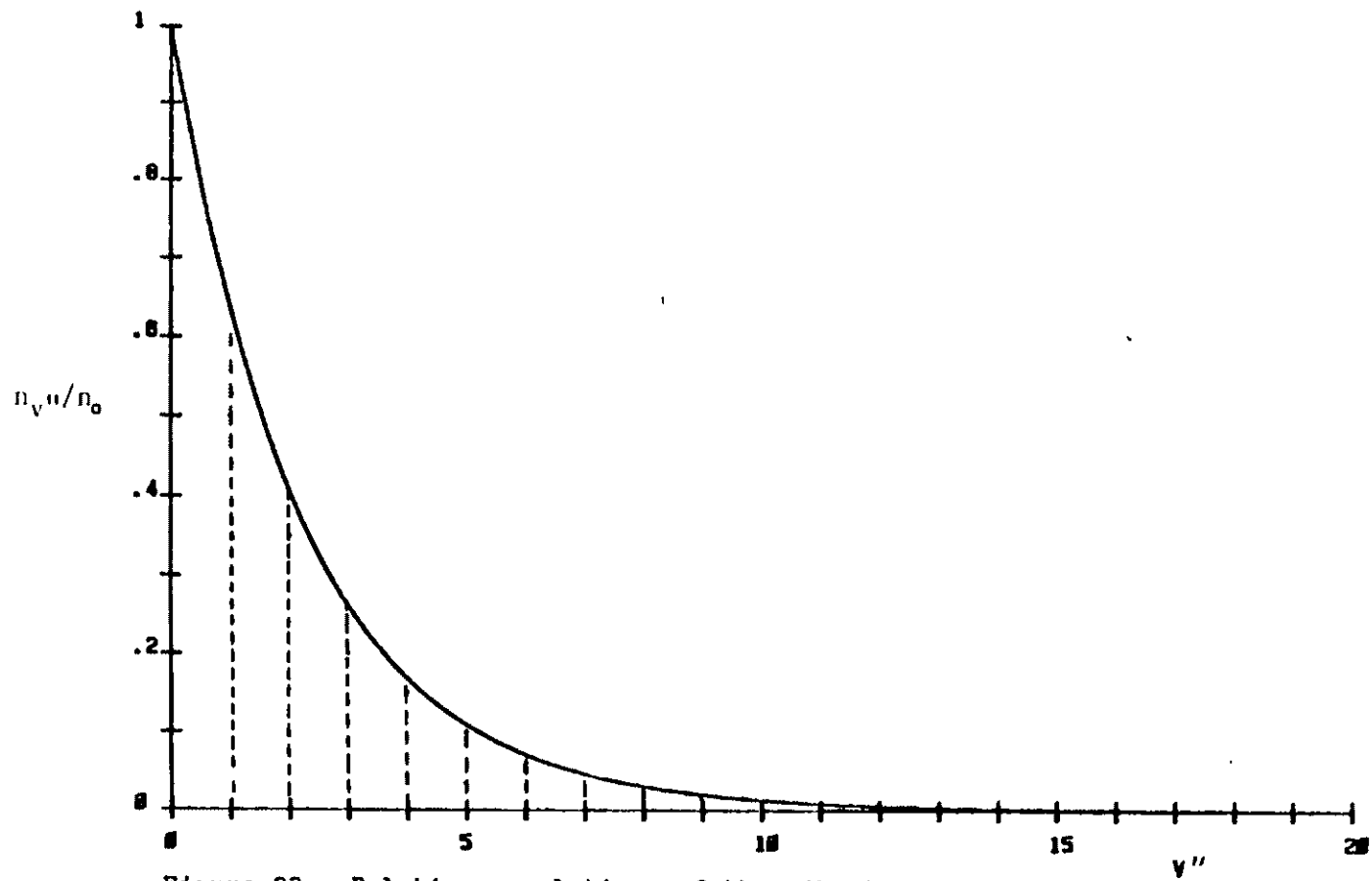


Figure 23. Relative populations of the vibrational energy levels for Na₂ gas at 500°K.

level v and the zero level. The zero-point energy can be left out, since to add this to the exponent would mean only adding a factor that is constant for all the vibrational levels (including the zero level).

The ordinates corresponding to the discrete values of the vibrational energy for the case of Na_2 are indicated by broken lines in Figure 23. The spacing between the lines becomes small at higher v (anharmonic oscillator) and $G_0(v)hc = \{G(v) - G(0)\}hc = 157.6732v - 0.7254v^2$. It is seen from this figure that the number of molecules in the higher vibrational levels falls off very rapidly.

The quantity $\exp[-(G_0(v)hc/kT)]$ give the relative density of molecules in the different vibrational levels referred to the density of molecules n_0 in state $v=0$. We have to consider that n is proportional, with the same factor of proportionality as before, to the sum of the densities in all the levels $n = n_v$, or the sum of the Boltzmann factors over all states, the so-called state sum (or partition function), given by

$$Q_v = 1 + \exp[-(G_0(1)hc/kT)] + \exp[-(G_0(2)hc/kT)] + \dots \quad (31)$$

Therefore, the density of molecules in the vibrational state v is

$$n_v = (n/Q_v) \exp[-(G_0(v)hc/kT)] \quad (32)$$

Successive terms in equation (32) decreased very rapidly, and we took 25 terms for the Na_2 ${}^1\Sigma_g^+$ state which was adequate.

Because of the low resolution of the monochromator, we

simplified the case by neglecting the thermal distribution of the rotational levels and assuming $J=0$ for all vibrational states.

To calculate the average density of sodium diatoms in vibrational level v , we integrated over space using cylindrical coordinates (see Figure 4.), and

$$N_v = \int_V n_v(r, \theta, z) d\tau \quad (33)$$

where N_v is total number of sodium diatoms in vibrational level v , $n_v(r, \theta, z)$ is the density of sodium diatoms in vibrational level v at the point (r, θ, z) , and $d\tau$ is an element of volume inside the heat-pipe.

Changing the density to pressure by using the ideal gas law, and combining equation (32).

$$\begin{aligned} N_v &= \int_V (P_{Na_2}/RT) N_A \exp(-(G_o(v)hc)/kT) Q_v^{-1} d\tau \quad (34) \\ &= (4\pi N_A/R) \int_0^{L_c} \int_0^{r_c} (P_{Na_2}/T) \exp(-(G_o(v)hc)/kT) Q_v^{-1} r dr dz \end{aligned}$$

where R is the gas constant and N_A is Avogadro's number and temperature T is a function of z and r (see equations (29) and (30)).

The average density of sodium diatoms in the vibrational level v is given by

$$\begin{aligned} \bar{n}_v &= N_v/V = N_v/2L_c\pi r_c^2 \quad (35) \\ &= (2N_A/r_c^2 L_c R) \int_0^{L_c} \int_0^{r_c} (P_{Na_2}/T) \exp(-(G_o(v)hc)/kT) Q_v^{-1} r dr dz \end{aligned}$$

where V is the volume of the heat-pipe in the vapor zone, L_0 is the half length of the oven, and r_0 is the radius of the heat-pipe.

Using Beer's law, equation (18), if we know the distribution function of density of the sodium dimers versus position and integrate point by point over the optical path, the absorption cross-section would be obtained.

$$\begin{aligned} \sigma_{\text{abs}}(\lambda) &= r_0^2 R / (4N_A) \ln(I_0^\lambda / I_t^\lambda) / & (36) \\ & \int_0^{L_0} \int_0^{r_0} P_{\text{Na}_2} / T \exp(-(G_0(v)hc) / kT) \cdot Qv^{-1} \, r dr \, dz \\ & = (5.4943314E-23 / S_2) \cdot \ln(I_0^\lambda / I_t^\lambda) \end{aligned}$$

where $S_2 = \int_0^{L_0} \int_0^{r_0} P_{\text{Na}_2} / T \exp(-(G_0(v)hc) / kT) \cdot Qv^{-1} \, r dr \, dz$,
 $L_0 = 16 \text{ cm}$, $r_0 = 1.27 \text{ cm}$,
 T is equation (26), and P_{Na_2} is equation (20).

To estimate the wavelengths and to match with the correct peaks in the experimental figures, we needed the values of the energy levels and the selection rule of sodium diatoms. If the Franck-Condon factor is non-zero, it implies that the transition is allowed between these two energy levels.

W. J. Stevens and M. M. Hessel and their co-workers provided a transition probabilities table for A-X transitions [22]. Even though the table includes the rotational transitions, the Franck-Condon factors are slowly varying functions of rotational level J and this table is still useful. P. Kusch and M. M. Hessels' published the Franck-Condon factor table for B-X transitions [23]. The entire C-X system is provided by R. D. Hudon [24] to be a reference of our data.

From Figure 10. to Figure 20., we measured the $I_0^\lambda / I_t^\lambda$ ratios at the wavelengths which correspond to the $v''=0$ progression and for

which the Franck-Condon factors for A-X, B-X, and C-X are not zero. For example, the peak number 47 of the B₄X curve in Figure 10. has X=17.98 cm. By using equation (16), we got the value of wavelength, 4891.2677Å and compared this value with other wavelengths which had been calculated by using equation (9) and two energy levels, v'' and v', are allowed transitions (the Franck-Condon factors are non-zero.). The wavelength 4896.02Å (v''=0 → v'=1) is the correct wavelength for the 47. We had measured I₀^λ/I_c^λ=6.65/2.93 and the absorption cross-section at wavelength 4896.02Å is 9.407Å². Finally, we used the Dec-10 computer to compute the cross-section from our experimental data. The absorption cross-sections of sodium dimers under different buffer gas pressures and temperatures are listed in next two pages:

		average temperature	
v'	wavelength (\AA)	646°K	678°K
4	6612.90	1.692	1.737
5	6563.53	2.049	1.844
6	6515.19	2.063	2.045
7	6467.85	2.128	2.553
8	6421.49	2.124	1.925
9	6376.08	2.242	2.210
10	6331.59	1.882	1.694
11	6288.00	1.973	2.280
12	6245.27	2.293	1.964
13	6203.40	1.457	1.759

Table 1. For $v''=0$, absorption cross-sections (\AA^2) of A_4X transitions for pressure of buffer gas, helium, 20 torr.

		average temperature			
v'	wavelength (\AA)	624°K	652°K	688°K	711°K
4	6612.90		1.370	2.099	1.590
5	6563.53		2.425	2.319	1.796
6	6515.19	2.608	2.321	2.603	1.942
7	6467.85	1.497	2.285	2.633	1.982
8	6421.49	1.998	1.828	2.354	1.802
9	6376.08	2.257	2.410	2.906	2.177
10	6331.59	2.028	2.095	2.606	2.065
11	6288.00	3.358	2.584	3.016	2.343
12	6245.27	3.274	2.136	2.880	2.291
13	6203.40	2.580	1.594	2.658	2.158

Table 2. For $v''=0$, absorption cross-sections (\AA^2) of A_4X transitions for pressure of buffer gas, helium, 30 torr.

		average temperature	
v'	wavelength (Å)	648°K	678°K
0	4925.67	7.780	6.544
1	4896.02	9.407	7.500
2	4867.09	9.662	7.280
3	4838.87	9.014	7.090
4	4811.33	9.307	6.840
5	4784.46	7.903	6.304
6	4758.26	6.645	5.981
7	4732.72	5.555	6.076
8	4707.82	5.394	

Table 3. For $v''=0$, absorption cross-sections (Å^2) of B \leftarrow X transitions for pressure of buffer gas, helium, 20 torr.

		average temperature			
v'	wavelength (Å)	624°K	652°K	688°K	711°K
0	4925.67	7.236	7.617	6.187	4.825
1	4896.02	11.45	10.26	7.289	5.056
2	4867.09	11.77	10.31	7.103	5.130
3	4838.87	10.09	9.345	6.625	4.799
4	4811.33	9.454	9.222	6.365	4.787
5	4784.46	8.658	8.193	5.926	4.287
6	4758.26	6.319	7.105	5.634	4.247
7	4732.72			5.304	4.118

Table 4. For $v''=0$, absorption cross-sections (Å^2) of B \leftarrow X transitions for pressure of buffer gas, helium, 30 torr.

		average temperature	
v'	wavelength (Å)	688°K	711°K
0	3405.74	0.425	0.139
4	3352.46	0.471	0.197
5	3339.69	0.544	0.157
6	3327.14	0.449	0.200
7	3314.79	0.614	0.215

Table 5. For $v''=0$, absorption cross-sections (Å^2) of C \leftarrow X transitions for pressure of buffer gas, helium, 30 torr.

CHAPTER V

DISCUSSION AND CONCLUSION

To measure the absorption cross-section, $\sigma_{\text{abs}}(\lambda)$, the usual practice is to let light pass through a certain length of uniform absorbing material, by operating a heat-pipe in "heat-pipe" mode. A relatively large amount of sodium would be used in the heat-pipe, and besides the optical path is difficult to measure. Here we used a different technique, and operated the heat-pipe in "non-heat-pipe" mode. The density of the sodium dimers became non-uniform over the optical path. By calculating the distribution function of density of the sodium dimers versus position and integrating point by point along the optical path, the $\sigma_{\text{abs}}(\lambda)$ was obtained (see equation (36)).

A K-type thermocouple (alumel-chromel) in the temperature range 530°F-2300°F has an error $\pm 0.75\%$. The error of the vapor pressure formula, equation (20), is related to the temperature (see Figure 21.). Combining these errors, the error of concentration of sodium dimer at 800°K ranges from +10.5% to -13% and its error at 623°K is +16% to -10%. The total systematic error is roughly estimated to be $\pm 20\%$.

The absorption cross-section for B \leftrightarrow X transitions decreased with increasing temperature (see Figure 24.) in approximately a linear fashion. The absorption cross-section, $\sigma_{\text{abs}}(\lambda)$ for A \leftrightarrow X transitions

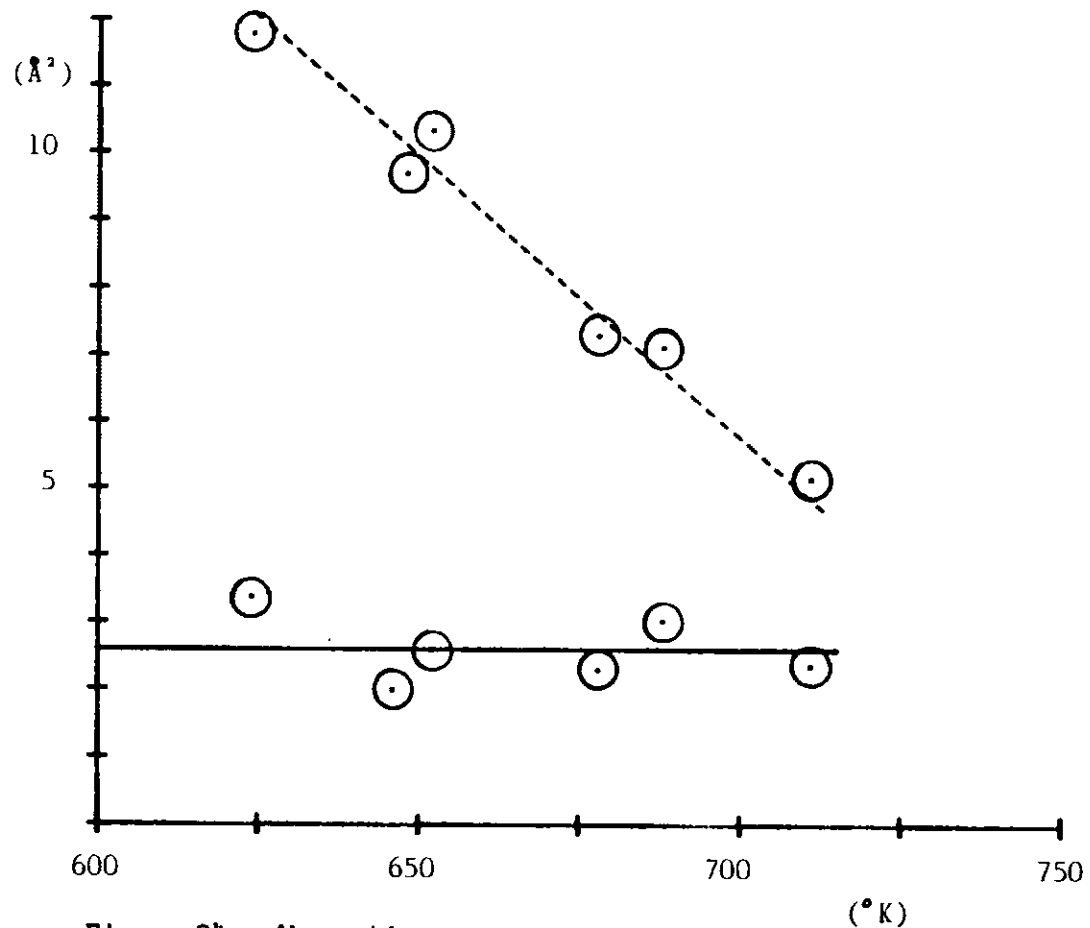


Figure 24. Absorption cross-section versus temperature. The points around the solid line are the absorption cross-section for A←X transitions at wavelength, 628.8 nm and the points around the dashed line are the absorption cross-section for B←X transitions at wavelength, 486.7 nm.

slightly decreased as temperature increases (also see Figure 24.). The measured $\sigma_{\text{abs}}(\lambda)$ was independent of the pressure of buffer gas, helium, (see Table 3., column 3, and Table 4., column 4.), because the thermal conductivity was independent of the pressure [5], and the changing the pressure should not have altered the temperature.

The overall absorption cross-section was a function of wavelength and also related to the Franck-Condon factor, $|\langle v' | v'' \rangle|^2$. ($\sigma_{\text{abs}}(\lambda) = |\langle v' | v'' \rangle|^2 / \lambda$, where λ is the wavelength of the absorbing photon determined by equation (9), and $|\langle v' | v'' \rangle|^2$ is the Franck-Condon factor given by equation (15).) We plotted the absorption cross-sections ($B \leftarrow X$) taken from the table 4. column 1 versus wavelength (see Figure 25.). In Figure 25., the absorption band has a (1%) bandwidth of 57nm, from 521.6nm to 464.6nm. The peak is at wavelength 4867.09Å which is the vibrational transition from $v''=0$ to $v'=2$ and also has the biggest Franck-Condon factor, $|\langle 0 | 2 \rangle|^2 = 0.212$ [23], in the $v''=0$ progression. The envelope of the absorption band for $B \leftarrow X$ transitions resembles a Gaussian absorption curve [25]. The full width at half maximum approximates to 28nm. The peak value decreases (see Figure 24.) and the wings widen as the temperature increases. It is difficult to estimate the bandwidth of $C \leftarrow X$ transitions and $A \leftarrow X$ transitions but in order of magnitude the full width at half maximum values are 15nm ($T_{\text{ave}}=688^\circ\text{K}$) and 60nm ($T_{\text{ave}}=652^\circ\text{K}$). The reason for the uncertainty is that the signal/noise ratio is small at both wavelength ranges.

Comparing our data with L. K. Lam, A. Gallagher and M. M. Hessels' data [8] and M. A. Henesian, R. L. Herbst and R. L. Byers' results [9], our results agree with the former group. L. K. Lam and

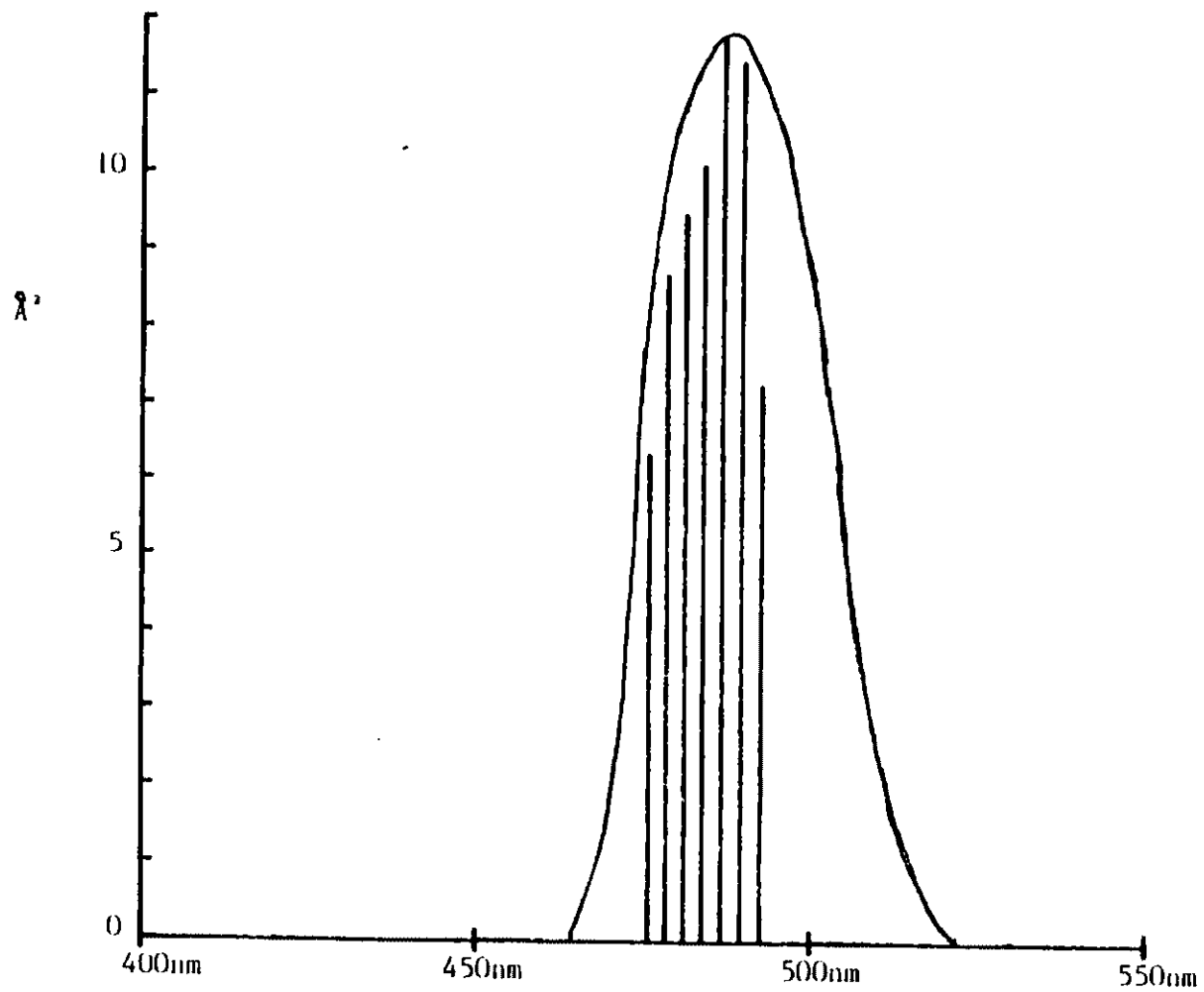


Figure 25. Plot of σ_{abs} (B-X) versus wavelength for Na_2 at $T_{\text{ave}}=624^{\circ}\text{K}$ for the transitions $v''=0$ to $v'=0 - 6$.

his partners obtained the value of the absorption cross-section at wavelength 670nm (A \leftarrow X transitions), $\sim 2.6 \cdot 10^{-16}$ cm², at temperatures $\sim 800^\circ\text{K}$. M. A. Henesian and his co-workers obtained $\sigma_{\text{abs}} = 3.00 \cdot 10^{-12}$ cm² at the same wavelength under the condition that the temperature of their oven was 600°C (873°K). There is a huge difference of 10^4 between of these two data. Our data indicate σ_{abs} is $2.26 \cdot 10^{-16}$ cm² (average value) at 651.5nm and according to reference [8], σ_{abs} is around $3.0 \cdot 10^{-16}$ cm². For σ_{abs} of the C \leftarrow X transitions at $T_{\text{ave}} = 688^\circ\text{K}$, our values are approximately 4.5 times bigger than Hudon's [24].

In conclusion the absorption cross-sections of the sodium dimers for the $v''=0$ progression in the red, visible and near ultraviolet have been measured and related to the Franck-Condon factors. The three peak values for the $v''=0$ progression A \leftarrow X transitions are 2.59 \AA^2 (average value), for the $v''=0$ progression B \leftarrow X transitions are 11.77 \AA^2 , and the $v''=0$ progression C \leftarrow X transitions are 0.6 \AA^2 ($T_{\text{ave}} = 688^\circ\text{K}$). The peak values occur at 628.8nm (A \leftarrow X), 486.7nm (B \leftarrow X), and 331.5nm (C \leftarrow X) respectively. The full width at half maximum values are A \leftarrow X, 60nm, and B \leftarrow X, 28nm, and C \leftarrow X, 15nm.

BIBLIOGRAPHY

- [1] C. G. Young, *Appl. Opt.*,5,pp.993-997,1966
- [2] W. L. Harries and W. E. Meador, *Space Solar Power Review*,4,pp.189-202,1983
- [3] B. Wellegehausen, *IEEE J. of Quantum Electronics*, QE-15,pp.1108-1130,1979
- [4] B. Wellegehausen, S. Shahdin, D. Friede, and H. Welling, *Appl. phys.*,13,pp.97-99,1977
- [5] W. L. Harries and J. W. Wilson, *Space Solar Power Rev.*, 2,pp.367-381,1981
- [6] W. L. Harries, *J. of Propulsion and Power*,1,pp.411-413,1985
- [7] M. Lapp and L. P. Harries, *J. Quantum. Spectry, Radative Transfer*,pp.169-179,1966
- [8] L. K. Lam, A. Gallagher, and M. M. Hessel, *J. chem. phys.*, 66,pp.3550-3556,1977
- [9] M. A. Henesian, R. L. Herbst, and R. L. Byer, *J. Appl. phys.*, 47,pp.1515-1518,1976
- [10] W. C. Stwalley and M. E. Koch, *Opt. Engineering*,19, pp.71-84,1980
- [11] M. Born and J. R. Oppenheimer, *Ann. d. physik* 84,457,1927
- [12] P. M. Morse, *phys. Rev.*,34,pp.57-64,1929
- [13] K. P. Huber and G. Herzberg: Molecular Spectra and Molecular Structure. IV. Constants of Diatomic Molecules, Van Nostrand Reinhold Comp.,N.Y.,1979
- [14] A.S. Davydov, Quantum Mechanics, Pergamon Press Ltd.,N.Y.,1965
- [15] C. R. Vidal and J. Cooper, *J. Appl. phys.*,40,pp.3370-3374,1976
- [16] S. W. Chi, Heat Pipe Theory and Practice, McGraw-Hill book Comp.,N.Y.,1976
- [17] K. Burns and K. B. Adams, *J. Opt. Soc. Am.*,42,pp.716-721,1952
- [18] R. P. Bauman, Absorption Spectroscopy, John Wiley & Sons, Ins.,N.Y.,1962

- [19] M. W. Zemansky, Heat and Thermodynamics, p.360, McGraw-Hill book Comp. inc.,N.Y.,1937
- [20] M. Sittig, Sodium,p.434, Renhold Pub. Corp.,N.Y.,1956
- [21] M. Sittig, Sodium,pp.478-486, Renhold Pub. Corp.,N.Y.,1956
- [22] W. J. Stevens and M. M. Hessel and P. J. Bertoncini and A. C. Wahl, J. chem. phys.,66,pp.1477-1482,1977
- [23] P. Kusch and M. M. Hessel, J. chem. phys.,68,pp.2591-2606,1978
- [24] R. D. Hudson, J. chem. phys.,43,pp.1790-1793,1965
- [25] W. L. Harries, Technical Report PTR 84-1 for NASA, Langley Research Center, p5, Jan. 1984

APPENDIX A

Assuming that the wavelength and the position X of the peaks in the spectrum obeyed the relationship $\lambda = aX^2 + bX + c$, and that the mercury light spectrum, wavelengths are $3,136.8391\text{\AA}$, $3,650.1533\text{\AA}$, and $4,046.5630\text{\AA}$, we measured the distances X of these peaks from the starting point. These distances were 3.64 cm, 19.56 cm, and 31.72 cm. The solutions for a , b , and c were $a=0.0124065$, $b=31.959235$, and $c=3,020.7489$.

Next the wavelengths $4,358.3277\text{\AA}$, $5,073.034\text{\AA}$, and $5,460.7348\text{\AA}$ were found to correspond to the distances 1.50 cm, 23.57 cm, and 35.43 cm. The solutions were $a=0.0089886$, $b=32.154454$, and $c=4,310.1209$.

For the wavelengths $5,769.5982\text{\AA}$, $5,790.6630\text{\AA}$, and $6,263.097\text{\AA}$, the distances were 5.18 cm, 5.84 cm, 20.02 cm. The solutions were $a=0.096799$, $b=30.829959$, and $c=5,607.2507$.

We list a table as follows:

wavelength range	a	b	c
300nm-420nm	0.0124065	31.959235	3,020.7489
430nm-550nm	0.0089886	32.154454	4,310.1209
560nm-680nm	0.096799	30.829959	5,607.2507

APPENDIX B

In the r direction

$$T_r'' + T_r' / r + (T_r'^2 / 2T_r^2 + \alpha^2) T_r = 0 \quad (\text{B-1})$$

Changing the variable:

Let $U = T_r' / T_r$, $T_r \neq 0$, and $T_r' \neq 0$ (temperature will not become zero.), then equation (B-1) becomes

$$U' / U + U + 1/r + U/2 - \alpha^2 / U = 0 \quad (\text{B-2})$$

Changing the variable again:

Let $W = rU$

$$W' + 3W^2 / 2r + \alpha^2 r = 0 \quad (\text{B-3})$$

let $W = 2rn' / 3n$ and $n \neq 0$

We have an exact Bessel's equation.

$$rn'' + n' + 3\alpha^2 rn / 2 = 0 \quad (\text{B-4})$$

$$n = C_1 J_0(\sqrt{3/2} \alpha r) + C_2 Y_0(\sqrt{3/2} \alpha r) \quad (\text{B-5})$$

C_1 and C_2 are two constants and C_2 is zero to keep the function from divergence. It follows:

$$W = 2rn' / 3n = \frac{2r}{3} \frac{dI_s ds}{J_0 dr}, \quad s = \sqrt{3/2} \alpha r$$

$$W = Ur \quad U = \frac{2}{3} \frac{dI_s ds}{J_0 dr}$$

$$U = T_r' / T_r \quad T_r = J_0^{2/3} (\sqrt{3/2} \alpha r) \quad (\text{let } C_1 = 1)$$

In the z direction

$$T_z'' + (T_z^2 / 2T_z^2 - \alpha^2) T_z = 0 \quad (\text{B-6})$$

Let $T_z = \exp(C^* z)$ and inserting into equation (B-6)

$$[C^{*2} - C^{*2} / 2 - \alpha^2] e^{C^* z} = 0, \quad e^{C^* z} \neq 0 \Rightarrow C^{*2} - C^{*2} / 2 - \alpha^2 = 0 \quad (\text{B-7})$$

So $C^* = \pm \sqrt{2/3} \alpha$

$$T_z = A^* \exp(\sqrt{2/3} \alpha z) + B^* \exp(-\sqrt{2/3} \alpha z) \quad (\text{B-8})$$

where A^* and B^* are constants.

the maximum temperature at the center of the heat-pipe.

$$\text{at } z=0, T_z = T_{\max} \Rightarrow A^* = -B^*$$

$$T_z = T_{\max} - A^* \sinh(\sqrt{2/3} \alpha z) \quad (\text{B-9})$$

where $A = 2A^*$. Values of A^* and α are given in Appendix C.

APPENDIX C

The heat-pipe was heated around 130 watts and filled with helium to 30 torr. After heating several hours, four temperature readings were obtained. They were 622.75°K, 611.45°K, 560.45°K, and 399.15°K. From this boundary condition, we would estimate three constants, T_{\max} , α , and A for equations (29) and (30). Since the thermocouples were directly contacted with the wall of the heat-pipe, $T_r(r=1.27 \text{ cm})=1$.

$$T=T_z T_r(r=1.27 \text{ cm})=T_z=[T_{\max}-A*\sinh(\sqrt{2/3}*z*\alpha)] \quad (C-1)$$

By using equation (C-1), The temperature at the center of the heat-pipe, $z=0 \text{ cm}$

$$T=T_{\max}=622.75^\circ\text{K} \quad (C-2)$$

To get the constants, A and α , we must use two temperature readings at $z=10.16 \text{ cm}$ and $z=17.46 \text{ cm}$ and equation (C-1) and solve it. The solution were $A=22.61898424$ and $\alpha= 0.209478879$ (see Figure 22.). These values were changed only by the input power.